DOI: 10.11835/j.issn.2096-6717.2026.050
开放科学(资源服务)标识码 OSID:

# 不同养护条件下琼脂改良砂土无侧限抗压强度及破坏机制

杨悦苓[1],覃长兵[1,2],CHIAN Siau Chen[3]
(1. 重庆大学 土木工程学院,重庆 400045; 2. 山区土木工程安全与韧性全国重点实验室,重庆 400045; 3. 新加坡国立大学 土木工程系,新加坡)

**摘 要:**传统砂土加固材料存在高碳排放和环境污染问题,亟待开发可持续替代方案。采用琼脂胶作为生物聚合物固化剂,以河南信阳级配不良河砂(SP)为对象,研究琼脂胶掺量(0.5%~2.0%,以粉末质量占干砂质量百分比计)、养护时间(3~28 d)和养护温度(20~60 ℃)对改良砂土无侧限抗压强度(UCS)的影响,并结合扫描电镜(SEM)探讨微观增强机制。结果表明:UCS随掺量增加显著提高,2%掺量试样28 d养护后UCS达638.5 kPa,为0.5%掺量的3.35倍;7 d养护即可达到28 d强度的90%以上,强度与残余含水率呈显著负相关;温度从20 ℃升至60 ℃时,温度每升高10 ℃,UCS平均增长11.78%。依据胶结状态归纳出6类破坏模式,高掺量(≥1.5%)充分养护试样呈脆性剪切破坏,低掺量(≤1%)短时养护试样呈渐进式破坏。此外,还探讨了颗粒包裹、孔隙填充和粒间桥接等微观增强机制。

**关键词:**琼脂胶改良砂土;抗压强度;扫描电镜;微观机制
**中图分类号:**TU44 **文献标志码:**A **文章编号:**2096-6717(XXXX)XX-0001-27

# Unconfined compressive strength and failure mechanisms of agar gum-treated sand under different curing conditions

*YANG Yueling[1], QIN Changbing[1,2], CHIAN Siau Chen[3]*
(1. School of Civil Engineering, Chongqing University, Chongqing 400045, China; 2. State Key Laboratory of Safety and Resilience of Civil Engineering in Mountain Area, Chongqing 400045, China; 3.Department of Civil Engineering, National University of Singapore, Singapore)

**Abstract:** Conventional sand reinforcement materials are associated with high carbon emissions and environmental pollution, necessitating sustainable alternatives. This study employs agar gum as a biopolymer binder to treat poorly graded river sand (SP) from Xinyang, Henan Province. The effects of agar gum content (0.5% - 2.0%, expressed as the mass percentage of agar gum powder to dry sand), curing time (3 d - 28 d), and curing temperature (20 ℃ - 60 ℃) on the unconfined compressive strength (UCS) of treated sand were investigated, with microscopic reinforcement mechanisms examined via scanning electron microscopy (SEM). The results show that UCS increases significantly with increasing agar gum content; the 28-d UCS of specimens with 2% agar gum reaches 638.5 kPa, which is 3.35 times that of specimens with 0.5% agar gum. Seven days of curing achieves over 90% of the 28-d strength, and UCS exhibits a strong negative correlation with residual moisture content.

**Received:** 2026-01-20
**Foundation items:** National Natural Science Foundation of China (No. 52578389)
**Author brief:** YANG Yueling (2001- ), main research interest: soil treated with biopolymers, E-mail: 202316021285t@stu.cqu.edu.cn.
QIN Changbing (corresponding author), professor, doctorial supervisor, E-mail: qinchangbing@cqu.edu.cn.

As curing temperature rises from 20 ℃ to 60 ℃, UCS increases by an average of 11.78% per 10 ℃ increment. Based on cementation states, six typical failure modes are identified: specimens with high agar gum content (≥1.5%) and sufficient curing (≥7 d) exhibit brittle shear failure, whereas those with low content (≤1%) and short curing (≤3 d) show progressive failure. Additionally, microscopic reinforcement mechanisms including particle coating, pore filling, and interparticle bridging are discussed.

**Keywords:** agar gum-treated sand; compressive strength; scanning electron microscope; microscopic mechanism

## 1 Introduction

Sand is one of the most widely available natural soil materials. Its loose structure and low cohesion pose significant challenges in engineering applications. Sand foundations are prone to liquefaction under dynamic loads, leading to piping and sand boils that can cause foundation instability. Under rainfall conditions, sand slopes are susceptible to instability, resulting in landslides and soil erosion. The low bearing capacity of sand can also cause uneven settlement, leading to cracks in buildings[1-2]. The geological hazards and engineering issues associated with natural sand have prompted researchers to continuously explore effective sand improvement techniques.

Sandy soil reinforcement technology has evolved from physical to chemical methods[3]. Traditional physical improvement methods primarily include foundation treatments such as dynamic compaction, gravel piling, and grouting, as well as reinforcement methods involving the addition of various grids, geotextiles, and single-strand fibers[4-5]. Although geogrids can temporarily enhance overall stability, their long-term performance is limited by material ageing[1]. Fiber reinforcement, such as polypropylene fibers, can improve the overall strength of soil, such as polypropylene fibers, increasing the shear strength of sand by 40% - 60%[6]. However, this does not fundamentally alter the loose structural characteristics of sand, and stress relaxation may occur under long-term dynamic loads[7]. Adding silty fines to the soil can change the cyclic liquefaction resistance of sand, but this effect is sensitive to changes in the content of silty fines, which may instead lead to a reduction in soil liquefaction resistance[8]. Chemical reinforcement technology primarily involves modifying sand by adding solidifiers, with inorganic cementitious materials such as cement, lime, and fly ash being the main representatives. Through hydration reactions, these materials form cementitious products that fill pores, significantly improving the engineering properties of sand. These inorganic solidifiers are widely applied in foundation reinforcement and road base engineering due to their low cost and excellent strength-enhancing effects[9-10]. However, their application has several drawbacks: the extensive use of cement leads to carbon dioxide and nitrogen oxide emissions, with carbon emissions per ton of cement production reaching 0.8 - 1.0 ton[11]. Currently, cement production accounts for 5% - 8% of global carbon dioxide emissions[12]. After solidification, the pH value of the soil can rise to 12 - 13, which may adversely affect groundwater and surrounding vegetation[13]. Such materials also increase soil brittleness, making the soil more prone to cracking and damage, thereby limiting their application in projects with high requirements for deformation coordination[14-15]. In recent years, there have been attempts to use organic polymeric materials such as polyacrylamide and epoxy resin for sand soil improvement, but these synthetic polymers present challenges such as slow degradation, potential toxicity, and high costs[16]. In this context, environmentally friendly improvement materials such as biopolymeric polymers have gradually become a research hotspot in the field of geotechnical engineering due to their sustainability, ecological friendliness, and unique bonding mechanisms.

Biopolymers offer numerous advantages, including widespread availability, low cost, low incorporation rates, and significant improvement effects. They can be biodegraded by microorganisms into water and carbon dioxide, thereby aligning with sustainable development requirements[17]. Biopolymers can be categorized into three major types based on their sources: plant-based (agar gum, guar gum), animal-

based (chitosan, casein), and microbial-based (xanthan gum, carrageenan). Research has shown that even small amounts of biopolymers can enhance the interparticle cohesion of non-cohesive soils, thereby significantly improving the bearing capacity of foundations[18]. Early studies primarily focused on the improvement effects of microbial-based biopolymers (such as xanthan gum). Chang et al. [19] mixed xanthan gum with standard sand and air-dried the samples at room temperature (20 ℃) for 28 days, finding that 1% xanthan gum could increase the unconfined compressive strength (UCS) of the samples from 0 to 0.88 MPa. Qureshi et al. [20] treated desert sand with xanthan gum and cured it in an oven at 45 ℃ for 28 days, finding that 1% xanthan gum resulted in a compressive strength of 1.076 MPa for the sand sample. Muguda et al. [21] mixed xanthan gum, guar gum, and soil samples with 80% non-cohesive soil content, and found that soil samples treated with 2% xanthan gum and guar gum had higher compressive strength than those treated with 8% cement. According to Chang et al. [19], the strength of xanthan gum-treated sand samples originates from the hydrogel matrix within the structure, which is formed by the drying of the polymer solution. During the curing process, the loss of water from the polymer solution causes hydrogel to shrink and harden, imparting it with a certain degree of strength. Simultaneously, the hydrogel encapsulates and connects soil particles, thereby enhancing the overall strength of the sample. Scholars have found that treating soil with biopolymers such as agar gum, carrageenan, and xanthan gum effectively improves the mechanical properties of various soil types by increasing the cohesive force between soil particles[16,22-23]. Table 1 shows a comparison of key characteristics of different biopolymers and the widely studied microbially induced carbonate precipitation (MICP) method. Scholars have recognized through extensive experiments the performance differences between various biopolymers: plant-based polymers such as guar gum and xanthan gum are cost-effective but have poor water resistance[24], while microbial-based polymers such as carrageenan provide high strength but are sensitive to cultivation conditions[25].

**Table 1　Comparison of agar gum with other biopolymers and MICP for sand stabilization.**

| Feature | Agar gum[16] | Xanthan gum[19-20] | Guar gum[21] | MICP[26] |
|---|---|---|---|---|
| Source | Red algae | Bacteria | Guar plant | Bacteria (urease) |
| Gelation mechanism | Thermo-gelation (sol-gel transition upon cooling) | Ionic cross-linking (mainly with $Ca^{2+}$) | Hydrogen bonding | Calcite precipitation |
| Curing requirement | Heating to >85 ℃, then cooling | Room temperature, air drying | Room temperature | Urea + $Ca^{2+}$ solution injection |
| Thermal reversibility | Yes (reversible) | No | No | No |
| Water resistance | Moderate to high (depends on concentration) | Poor (swells in water) | Poor (swells in water) | High (insoluble calcite) |
| Strength gain mechanism | Dense gel network, particle coating, bridging | Hydrogel matrix shrinkage | Hydrogen bonding networks | Crystal bridging and pore filling |
| pH stability | Good (stable 4-10) | Moderate | Moderate | High (alkaline) |
| Key limitation | Requires heating for initial dissolution | Weak water resistance; slow curing | Weak water resistance | ammonia release; complex bio-treatment |

Compared with xanthan gum and guar gum, agar gum exhibits unique thermo-gelation behavior that allows rapid gel formation upon cooling, producing a uniform and dense gel network without requiring prolonged air drying. Unlike MICP, which involves complex bio-culturing and may release ammonia, agar gum is a simple, environmentally friendly additive that can be easily mixed with sand. Specifically, agar gum forms high-strength gels at 30 ℃ - 40 ℃ and exhibits excellent thermal reversibility (enabling potential recycling and reuse, a feature not available in other biopolymers or MICP), along with shear thinning, wetting properties, interfacial tension, and good pH stability. Smitha found that 0.5% agar gum could increase the cohesion of sand by 15 times, laying the foundation for the application of agar gum in sand engineering[16].

Regarding the soil improvement effects of agar gum, Jang et al. [23] characterized agar gum used for soil improvement by studying its contact angle,

viscosity, and other properties. Studies on the shear strength, compressive strength, and other static properties of soil treated with agar gum biopolymers have been conducted by relevant scholars. Khatami et al. [27] found through triaxial compression tests that the addition of agar gum and starch effectively improved the cohesion and stiffness of treated sand. Chang et al. [28] found through immersion tests that thermal treatment is a necessary and effective condition for using thermosetting biopolymers such as agar gum and carrageenan to treat soil. The content of biopolymers, moisture content, and soil type are important parameters influencing the reinforcement behavior of thermosetting biopolymer soil treatment. Smitha and Rangaswamy[29] validated the potential of this material in reducing pore water pressure and enhancing dynamic properties and analyzed the effects of parameters such as agar gum concentration, curing time, and strain amplitude.

Current research primarily focuses on the extent to which biopolymers improve the engineering properties of soil, such as shear strength, compressive strength, and permeability. However, there is no systematic conclusion yet on the optimization effects of agar gum-treated sand under different curing conditions, such as concentration of agar gum, curing time, and curing temperature. Additionally, existing studies have primarily focused on macroscopic mechanical properties, lacking in-depth exploration and systematic classification of the failure mechanisms of cemented sand, and have not thoroughly explained the microscopic reinforcement mechanisms of agar gum on sand[30-31]. The following critical gaps remain unaddressed:

(1) Material scope. Most biopolymer studies employ standard silica sand (e. g., Ottawa sand, Fujian sand), whereas ordinary river sand—naturally sourced from riverbanks and used in this study to reflect realistic reinforcement performance—has received little attention. The particle morphology, mineralogy, and surface chemistry of river sand differ from standard sands, potentially affecting biopolymer adhesion and reinforcement efficiency.

(2) Systematic optimization. Although individual effects of biopolymer concentration, curing time, and temperature have been reported, no study has systematically investigated the effects of these three factors on agar gum-treated sand, particularly the identification of optimal curing windows for practical engineering.

(3) Failure mechanism classification. Existing studies on biopolymer-treated sand predominantly report stress-strain curves and strength values, but a systematic classification of failure modes (e. g., Y-type, X-type, sliding, petal-type) and their linkage to microscopic gel distribution and moisture state is lacking.

To fill these gaps, this study uses agar gum as the primary soil reinforcement agent, with river sand from Xinyang, Henan Province, as the experimental material. Through UCS tests, the stress-strain characteristics and peak compressive strength of treated sand under different agar gum content and curing conditions were obtained. The fracture failure characteristics of the specimens under different conditions were analyzed and combined with scanning electron microscopy (SEM) images to conduct an in-depth study on the microstructural characteristics of agar gum-treated sand. The adhesion behavior of polymers on sand particle surfaces and the evolution patterns of pore structures were investigated to explore the mechanical mechanisms of agar gum polymer reinforcement of sand.

## 2 Materials

### 2.1 Sand

The sand used in this study was river sand from Xinyang, Henan Province. By simulating the particle size distribution of soil in highly liquefiable areas, sand samples corresponding to low-graded sand (SP) under the unified soil classification system were prepared, as shown in Fig. 1. Sieving tests were conducted on the graded sand to obtain the grading curves of the sand samples, as shown on Fig. 2. Detailed physical parameter tests were conducted on the graded sand to determine the basic physical properties of the sand samples, as shown in Table 2.

Fujian standard sand (a widely used type of standard sand) is typically a well-graded quartz sand (SW) with rounded particles, whereas the Xinyang River sand is poorly graded (SP, $C_u = 2.37$) with sub-angular to sub-rounded particles, predominantly

**Fig. 1　Graded sand sample**

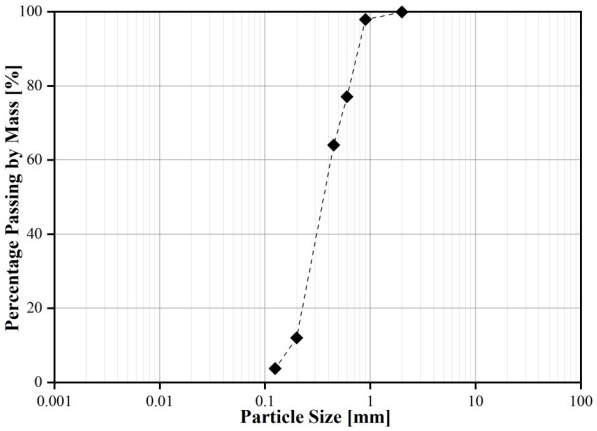


**Fig. 2　Grading curve of sand**

composed of quartz with minor percentages of feldspar and mica. SP sands are common in natural riverbeds, beaches, and aeolian deposits, making the findings directly relevant to such liquefaction-prone environments. However, the results may not be directly transferable to well-graded sand (SW) or sand with significant fines, and caution should be exercised when extrapolating to other conditions.

### 2.2　Biopolymer

The experiment used agar gum, an environmentally friendly plant-based biopolymer, as a soil conditioner. Agar gum is typically a polysaccharide extracted from several types of red algae, with a chemical structure formed by polysaccharides linked to galactose molecules, as shown in Fig. 3. Agar gum processed into powder form, as shown in Fig. 4(a), is widely used in various fields such as food, cosmetics, research, and industry. Agar gum is a water-soluble biopolymer that dissolves easily in boiling water and exhibits thermal gelation properties, meaning it forms a gel state when the temperature drops below a specific threshold. Therefore, when an agar gum-containing aqueous solution is heated above 85 ℃, it gradually dissolves and remains in a sol state, as shown in Fig. 4(b). Its diluted solution remains liquid at 45 ℃, and when the temperature drops below a specific threshold (generally below 37 ℃), it gradually turns into a compact gel, as shown in Fig. 4(c). Typically, agar gum powder dissolves in water at a temperature of approximately 85 ℃ - 90 ℃ and transforms into a gel at a temperature of approximately 32 ℃ - 45 ℃. Therefore, agar gum solutions always exist in a gel state at room temperature (25 ℃). Agar gum possesses high mechanical strength and can generate greater cohesive and adhesive forces between soil particles. Thus, when heated agar gum solutions in the sol state are injected into the ground, they gradually cool to a certain temperature and transform into agar gum. The gel formed by agar gum increases the cohesive force between soil particles, reduces effective stress, and prevents an increase in pore water pressure. Additionally, the strength of the soil increases with the concentration of agar gum after injection. Higher agar gum concentrations result in a denser gel network in the soil, reducing the size of the gaps between soil particles and enhancing the soil′s compressive strength. In this study, agar gum powder was mixed with distilled water to prepare an agar gum solution, which was then heated to dissolve the powder, resulting in a polymer solution in the form of a soul. The agar gum concentration was defined as the weight ratio of agar gum powder to dry sand.

**Table 2　Physical properties of the soil**

| Soil classification | Specific gravity $G_s$ | Maximum density/(g/cm$^3$) | Minimum density/(g/cm$^3$) | $D10$/ mm | $D30$/ mm | $D60$/ mm | $C_u$ | $C_c$ |
|---|---|---|---|---|---|---|---|---|
| SP | 2.68 | 1.53 | 1.34 | 0.18 | 0.29 | 0.43 | 2.37 | 1.04 |

### 2.3　Sample preparation

The preparation process for the test specimens in this study was carried out in accordance with the *Standard for Geotechnical Testing Methods* (GB/T 50123—2019)[32]. Specimens for the unconfined compression strength test were made from poorly graded sand with relative density 30% and dimensions 50 mm diameter and 100 mm high. The relative density

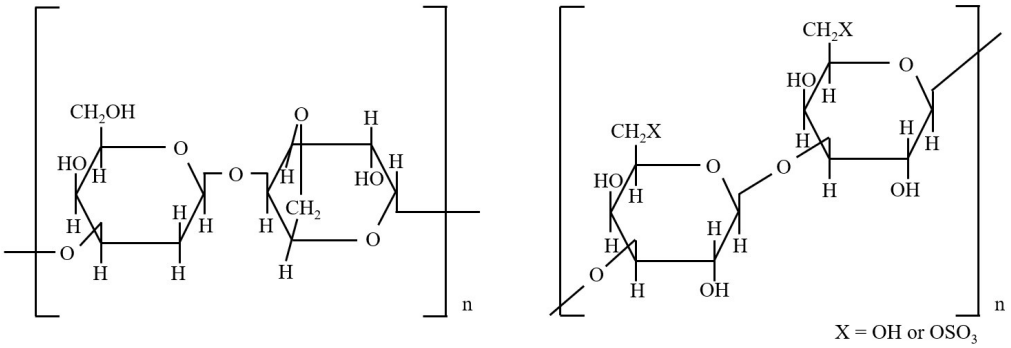


**Fig. 3 Chemical structure of agar gum**

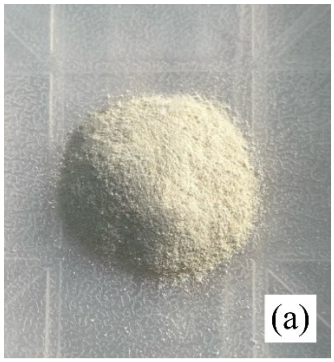


(a) Powdered agar gum

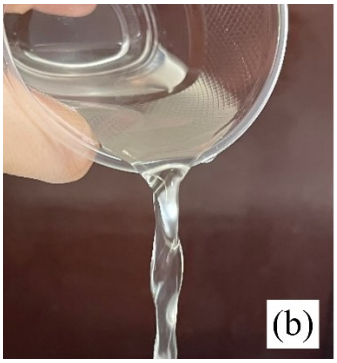


(b) Agar gum sol

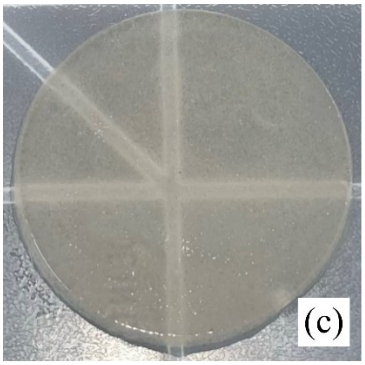


(c) Gelatinous agar gum

**Fig. 4 Agar gum in different states**

of 30% represents easily liquefiable loose sand. The specimens were prepared using the wet mixing method. Prior to specimen preparation, the soil sample was dried in an oven at 105 ℃ for 24 hours. First, the agar gum biopolymer in powder form was dissolved to achieve the desired concentration. The required agar gum content was calculated as a percentage of the mass of dried sand. A certain amount (0.5%, 1%, 1.5%, 2%) of agar gum powder was added to water (to achieve an initial moisture content of 25.3% in the sample), mixed thoroughly, and heated until the agar gum completely dissolved in the water to form a semi-viscous solution, as shown in Fig. 5(a)-(b). The initial moisture content of 25.3% was selected based on preliminary tests over a range of 20% – 35%: values above 30% caused demolding difficulties and gel segregation, while values below 22% led to poor workability and non-uniform mixing. The 25.3% value (≈75% of saturation) provided optimal workability and was adopted for all tests. To ensure uniform distribution of agar gum using manual mixing, the dry sand was preheated to 60 ℃ for 2 h, and the agar gum solution was heated to 90 ℃ then cooled to 60 ℃. The entire mixing process was conducted on a heating plate maintained above 60 ℃. The preheated sand was first folded and turned over 30 times with a spatula, then continuously stirred for two minutes until the mixture exhibited a uniform dark yellow color with no dry sand or gel lumps, as shown in Fig. 5(c). The relative density of 30% in the mold was equivalent to a dry density of the specimen equal to 1.45 g/cm$^3$. After mixing, the gel-soil mixture was evenly layered into a cylindrical mold, with each layer 3.33 cm high, as shown in Fig. 5(d). The layers were scraped at the interface, and a lubricant was applied to the inner wall of the mold before filling to facilitate demolding. After a few minutes, the sample inside the mold cooled and solidified, and the specimens were removed from the mold, as shown in Fig. 5(e). All demolded specimens were placed in an oven to provide uniform cur-

ing conditions, as shown in Fig. 5(f). The oven was set at the target temperature (20 ℃, 40 ℃, or 60 ℃) with no additional humidity control; the relative humidity inside the oven was measured to be 15% – 25% (ambient laboratory conditions) using a hygrometer. No humidification or dehumidification was applied. The specimens were weighed before and after curing to record changes in moisture content. The wet mixing method was adopted to ensure uniform distribution of agar gum in the soil samples. This approach addressed the limitation of the dry mixing method, where adding water to powdered soil within minutes under heating conditions prevented complete dissolution of agar gum. In the UCS test, sand samples with different agar gum contents (0.5%, 1%, 1.5%, 2%) cured under four different curing times (3, 7, 14, and 28 days) and different agar gum concentrations (0.5%, 1%, 1.5%, and 2%). Additionally, samples with a 2% agar gum concentration cured for 7 days at different oven temperatures (20 ℃, 40 ℃, and 60 ℃) were also tested. Consistency of curing conditions for treated samples was ensured by measuring the moisture content of samples.

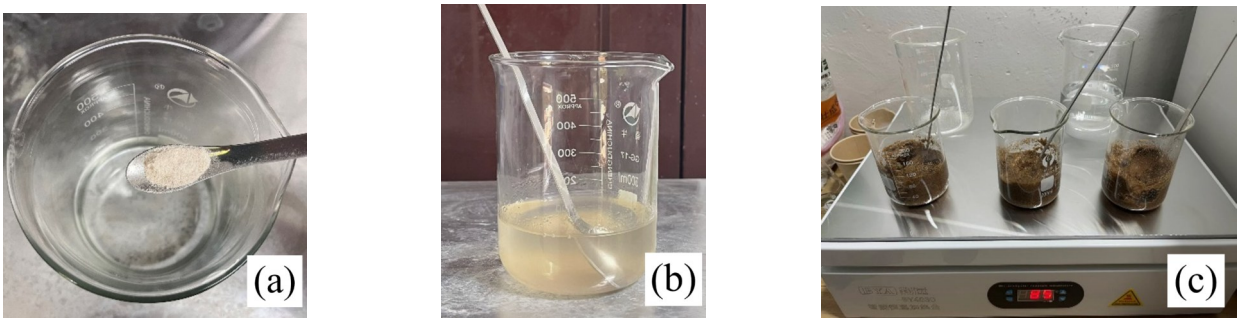


(a) Adding agar gum powder into clean water　(b) Heating the agar gum-water mixture　(c) Pouring hot agar gum solution into the dry sand and mixing them

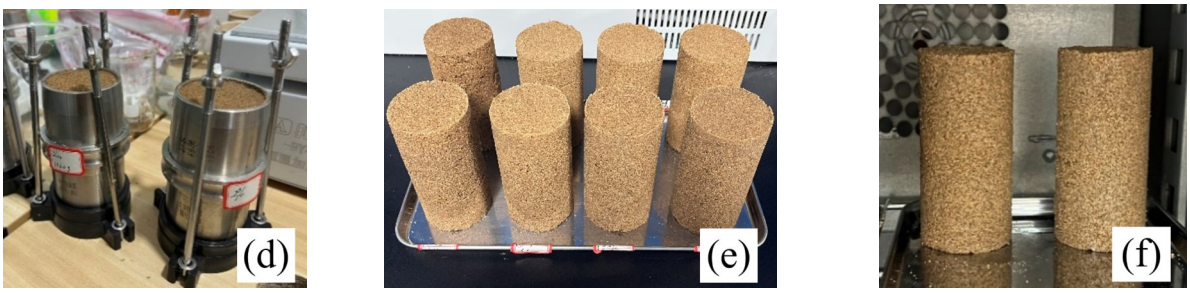


(d) Placing the mixture into the mold　(e) Removing the samples from the mold after cooling　(f) Curing the samples in an oven

**Fig. 5　Sample preparation process**

## 3　Methodology

### 3.1　Testing plan

The effects of different sample concentrations, curing time, and curing temperature on the UCS and final moisture content of agar gum-treated sand were investigated. To study the effects of these conditions on the microstructure of agar gum-treated sand, SEM testing was performed on samples prepared under the same conditions.

First, multiple preliminary experiments were conducted on agar gum-treated sand with different moisture contents, considering key factors such as specimen strength, workability, and subsequent research. In the following studies, the relative density Dr of the specimens was controlled at 30%, and the moisture content of the specimens was controlled at 25%, i. e., $W_{sol}/W_s \times 100 = 25$, where $W_{sol}$ represents the mass of the agar gum solution and $W_s$ represents the mass of the dry soil. Subsequently, the effects of agar gum content, curing time, and curing temperature on the UCS of agar gum-treated sand were investigated.

For the UCS test, the agar gum concentration was set at 0.5%, 1.0%, 1.5%, and 2.0%. This range was selected based on the feasible interval for

**Table 3 Testing plan**

| Experiment | Relative Density /% | Solution Content, ($W_{sol}/W_s$)/% | Curing temperature /℃ | Curing time /days | Agar gum concentration, ($M_a/M_s$) /% |
|---|---|---|---|---|---|
| UCS | 30 | 25 | 20 | 7 | 2 |
| | | | 40 | 3 | 0.5/1.0/1.5/2.0 |
| | | | 40 | 7 | 0.5/1.0/1.5/2.0 |
| | | | 40 | 14 | 0.5/1.0/1.5/2.0 |
| | | | 40 | 28 | 0.5/1.0/1.5/2.0 |
| | | | 60 | 7 | 2.0 |
| SEM | 30 | 25 | 20 | 7 | 2.0 |
| | | | 40 | 3 | 0.5/1.0/1.5/2.0 |
| | | | 40 | 7 | 0.5/1.0/1.5/2.0 |
| | | | 40 | 14 | 0.5/1.0/1.5/2.0 |
| | | | 40 | 28 | 0.5/1.0/1.5/2.0 |
| | | | 60 | 7 | 2.0 |

effective dissolution and gelation of agar gum in water. Preliminary tests showed that when the concentration exceeded 2.0%, the solution viscosity became excessive, leading to non-uniform mixing with sand and uneven gel distribution within soil pores; therefore, concentrations above 2.0% were not considered. This gradient design aimed to identify the optimal concentration range that balances construction feasibility and reinforcement effectiveness. To evaluate the effect of curing temperature on the gelation process and subsequent strength development, three levels (20 ℃, 40 ℃, and 60 ℃) were selected; 20 ℃ represents typical room temperature conditions and the ground surface temperature in most regions during spring and autumn; 40 ℃ and 60 ℃ simulate the high-temperature environment that the material may experience in summer or in specific regions (e.g., sun-exposed ground surfaces). Four curing times (3, 7, 14, and 28 days) were set to capture strength growth pattern over time, evaluating both early-stage strength and long-term stability, and to provide a basis for determining the appropriate curing period in engineering practice. Weight tests were conducted before and after curing to determine changes in moisture content, and representative samples were selected for subsequent SEM testing to investigate microstructural reinforcement mechanisms. Table 3 outlines the experimental plan.

### 3.2 UCS test

The unconfined compressive strength is an important indicator of soil mechanical properties. The results of UCS tests can reflect parameters such as soil compressive strength, elastic modulus, and residual strength, making them commonly used in studies aimed at improving soil mechanical properties. In this study, the YZM-II multifunctional pavement material strength testing machine was used to conduct UCS tests on each sample at a displacement rate of 2.4 mm/min, as specified in the Chinese standard GB/T 50123-2019[32] for unconfined compression tests. The testing equipment is shown on Fig. 6. During the test, the sample was placed at the center of the lifting plate, as shown in Fig. 7.

**Fig. 6 YZM-II multifunctional road surface material strength testing machine**

The UCS test procedure is as follows: (1) Place the specimen on the lifting plate, start the machine to slowly raise the lower pressure plate until the top of the specimen just contacts the upper pressure plate. At this point, the axial force gauge displays a read-

**Fig. 7　UCS test on agar gum-treated sand sample**

ing. Then, zero the readings of the axial displacement gauge and axial force gauge. (2) Begin the test by slowly raising the lower loading plate to apply load to the specimen until it is destroyed. During the test, record the axial displacement and axial stress readings, and take photographs at regular intervals to document the specimen's failure process. After the test, photograph and record the final failure state of each specimen. Each group of specimens should include three parallel specimens, and the average value should be taken as the result for analysis to reduce experimental error. (3) Plot the axial stress-axial strain relationship curve based on the test data. Take the axial stress corresponding to the peak point on the curve as the compressive strength of the specimen; if the curve does not have a distinct peak point, take the axial stress corresponding to 15% strain as the compressive strength value.

Previous experiments have not investigated the UCS of non-cohesive sand. An attempt was made to prepare samples using untreated sand in a mold, but due to extremely low cohesion, the samples could not be formed into cylinders, making it impossible to conduct UCS tests on untreated sand. All other samples were successfully formed and tested. As a reference, based on published data for similar poorly graded loose sand (SP), the internal friction angle typically ranges from 25° to 30° and the cohesion is negligible (close to 0 kPa)[33]. This provides a baseline for evaluating the improvement effect of agar gum treatment. At the end of each UCS test, photographs were taken of the treated samples with different agar gum concentrations and curing times to investigate the effects of these factors on the failure modes of the samples under compression and to identify the typical failure modes of the samples under compression. Three specimens were prepared and tested for each combination of agar gum concentration, curing time, and curing temperature. The UCS values reported in Section 4.1 are the mean of the three measurements. Data dispersion was assessed by calculating the standard deviation (SD) and the coefficient of variation (CV = SD/mean × 100%). Across all test conditions, the CV values ranged from 1.2% to 8.7%, indicating good repeatability of the experimental results.

### 3.3　Scanning electron microscope imaging

Imaging was performed using a ZEISS EVO 18 scanning electron microscope. After curing, a representative block (approximately 1　cm × 1　cm × 2　mm) was cut from the central region of each cylindrical specimen using a fine wire saw and a sharp blade. The block was carefully broken along its weak plane into smaller fragments (height ≤5　mm) to expose a fresh fracture surface with minimal disturbance, then mounted on an aluminum stub using conductive adhesive, and loose particles were removed. Gold coating was applied using a small ion sputter coater to enhance conductivity. The specimen was placed in the sample chamber under low vacuum, and images were captured at magnifications of 40×, 70×, 120×, and 300×.

## 4　Results and discussion

### 4.1　UCS test results

4.1.1　Effects of agar gum biopolymer concentration

The stress-strain curves of agar gum-treated sand at different concentrations and curing times are shown in Fig. 8. This figure shows that the stress of agar gum-treated sand at all concentrations and curing times first increased and then decreased with increasing axial strain. At a low agar gum concentration of 0.5%, the stress-strain curve patterns are less consistent, likely due to the agar gum not being uniformly distributed in the sand at low concentrations, as shown in Fig. 8(a). The stress-strain

growth trends of agar gum-treated sand samples at 1% agar gum concentration are similar, generally exhibiting strain softening behavior, as shown in Fig. 8 (b). When the agar gum content is higher, reaching 1.5% and 2%, the stress-strain curves of samples at different curing times exhibit consistent patterns, showing a more pronounced strain softening type, along with distinct peak strength and post-peak stress decline phenomena, as shown in Fig. 8(c), (d). At higher agar gum concentrations, the post-peak stress-strain curve of the samples changes more gradually, exhibiting a certain degree of ductile failure.

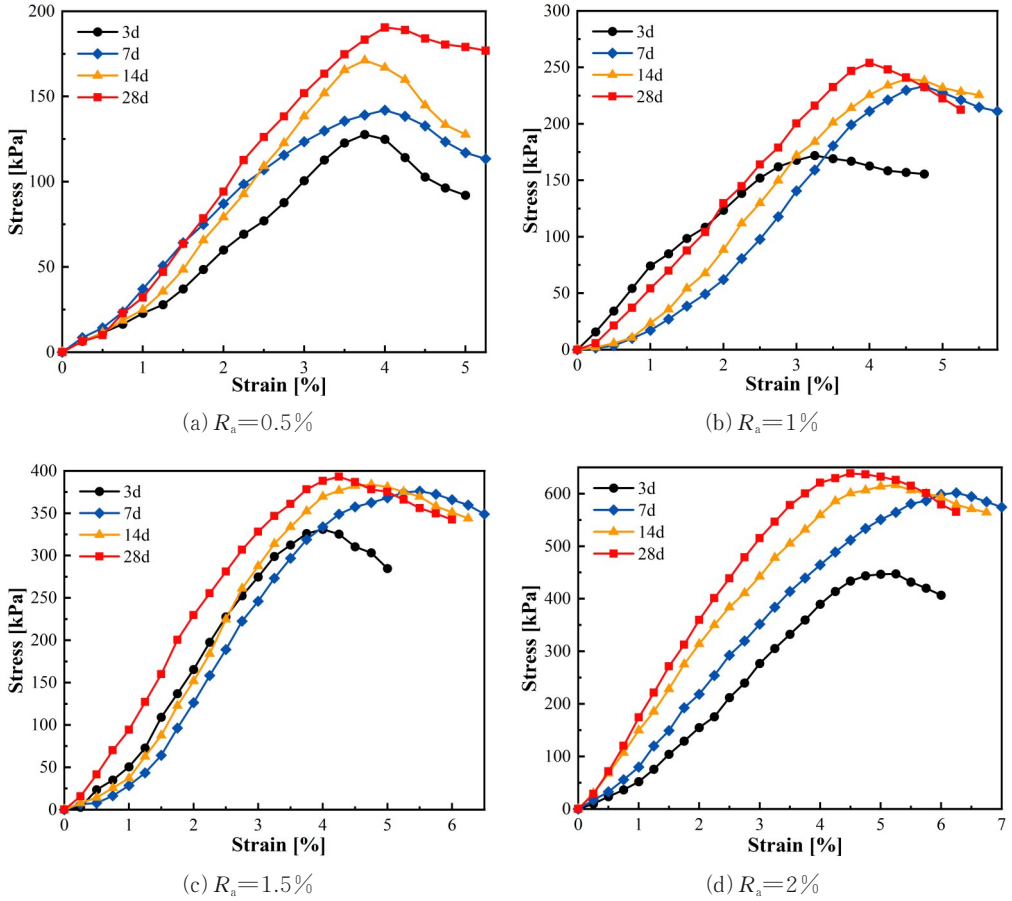


**Fig. 8 Axial stress-strain curves of agar gum-treated sand with different agar gum concentrations under different curing times**

Typically, the peak value of the axial stress-strain curve of the sample is taken as the UCS value. If the sample does not have a peak, the stress at 15% strain is taken as its UCS value. In the current study, all agar gum-treated samples exhibited distinct peaks and failed before reaching 15% strain. Untreated sand lacks cohesion to form a sand column, so its UCS cannot be measured. However, after treatment with low-concentration agar gum, cylindrical samples can be formed for testing. As shown in Fig. 9, the UCS value of the sample with 0.5% agar gum content after 3 days of curing is 127.69 kPa, indicating that agar gum treatment can impart a certain degree of stiffness and cohesion to non-cohesive sand.

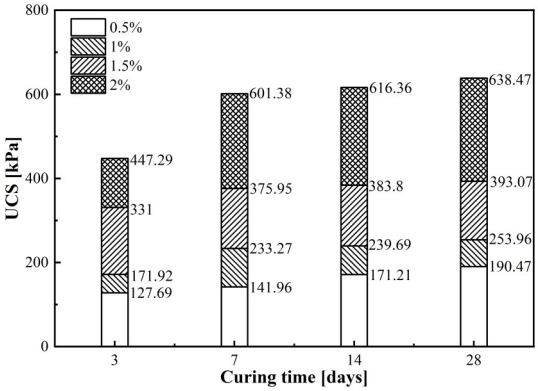


**Fig. 9 UCS of agar gum-treated sand at different concentrations and curing times**

At all curing times, samples with a 2% agar gum content consistently showed significantly higher UCS than those with 0.5% and 1% agar gum-treated sand. As shown in Fig. 9, after 28 days of curing, the 2% agar gum-treated sand exhibited the highest UCS, reaching 638.47 kPa. Following

closely behind were the sand samples with the same agar gum concentration cured for 14 days, with a peak UCS of 616.36 kPa. It can also be observed that the UCS of agar gum-treated samples stabilized at around 7 days and further increases in curing time resulted in only minor increases in UCS. Agar gum-treated sand after seven days of curing can achieve approximately 90% of the strength reached after 28 days.

The UCS increased with the increase in agar gum content at all curing times, indicating that agar gum content is an important factor influencing the compressive strength of treated sand. Both low agar gum content (0.5%, 1%) and high agar gum content (1.5%, 2%) enhanced the UCS of sand to some extent, but the improvement effects vary with different agar gum contents. As shown in Fig. 10, increasing agar gum content at low agar gum content does not significantly enhance the compressive strength of sand. At a curing time of 3 days, increasing the agar gum content from 0.5% to 1% resulted in a 0.34-fold increase in the compressive strength of the samples, and at a curing time of 28 days, the increase was 0.33-fold, with consistent growth patterns. At high addition levels, increasing the agar gum content significantly improves the compressive strength of sand. At a curing time of 7 days, the compressive strength of sand treated with 2% agar gum reached 601.38 kPa, which is 0.6 times higher than the compressive strength of sand treated with 1.5% agar gum at the same curing time (375.95 kPa). When the curing time was 28 days, increasing the agar gum content from 1.5% to 2% resulted in a 0.62-fold increase in the compressive strength of the samples, consistent with the trend observed at a curing time of 7 days. As shown in Fig. 10, the trend of strength changes caused by concentration variations is largely independent of curing time. At high addition rates, increasing agar gum concentration resulted in a greater increase in sample strength.

4.1.2　Effects of residual moisture content and curing time

The relationship between the UCS and moisture content of sand treated with agar gum at different curing times and agar concentrations is shown in Fig.

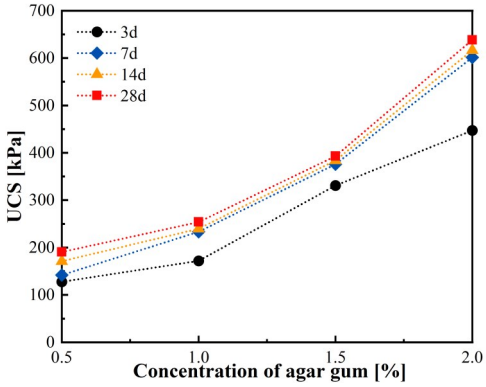


**Fig. 10　Variation of UCS of agar gum-treated sand at different curing times under different concentrations**

11. At the start of curing, all samples had the same initial moisture content. As the curing time increased, the residual moisture content of samples at all agar concentrations gradually decreased, and the UCS correspondingly increased. After 14 days of curing, the UCS and residual moisture content of samples at all concentrations basically stabilized. As shown in Fig. 11(c)-(d), after 7 days, the increase in UCS of the high-concentration (1.5% and 2%) samples slowed down. Between 14 and 28 days, the compressive strength of 1.5% agar gum-treated sand increased by 2%, and the residual moisture content decreased by 4.9%; the UCS of the 2% agar gum-treated sand increased by 3.6%, and the residual moisture content decreased by 2.1%. As shown in Fig. 11(a), the compressive strength of the low-concentration (0.5%) samples increased more significantly with increasing curing time. The compressive strength and residual moisture content changes of the samples with high-concentration were more stable than those of low-concentration samples. As shown in Fig. 11(a),(d), at the same curing time, the residual moisture content of high-concentration samples was always greater than that of low-concentration samples, and as the curing time increased, the difference in residual moisture content gradually decreased. Furthermore, at any curing time, high-concentration samples showed greater compressive strength than low-concentration samples.

Systematic analysis revealed that the residual moisture content of samples at 3 days of curing showed little variation across different concentrations. Therefore, the average moisture content for each curing time group was calculated to observe the

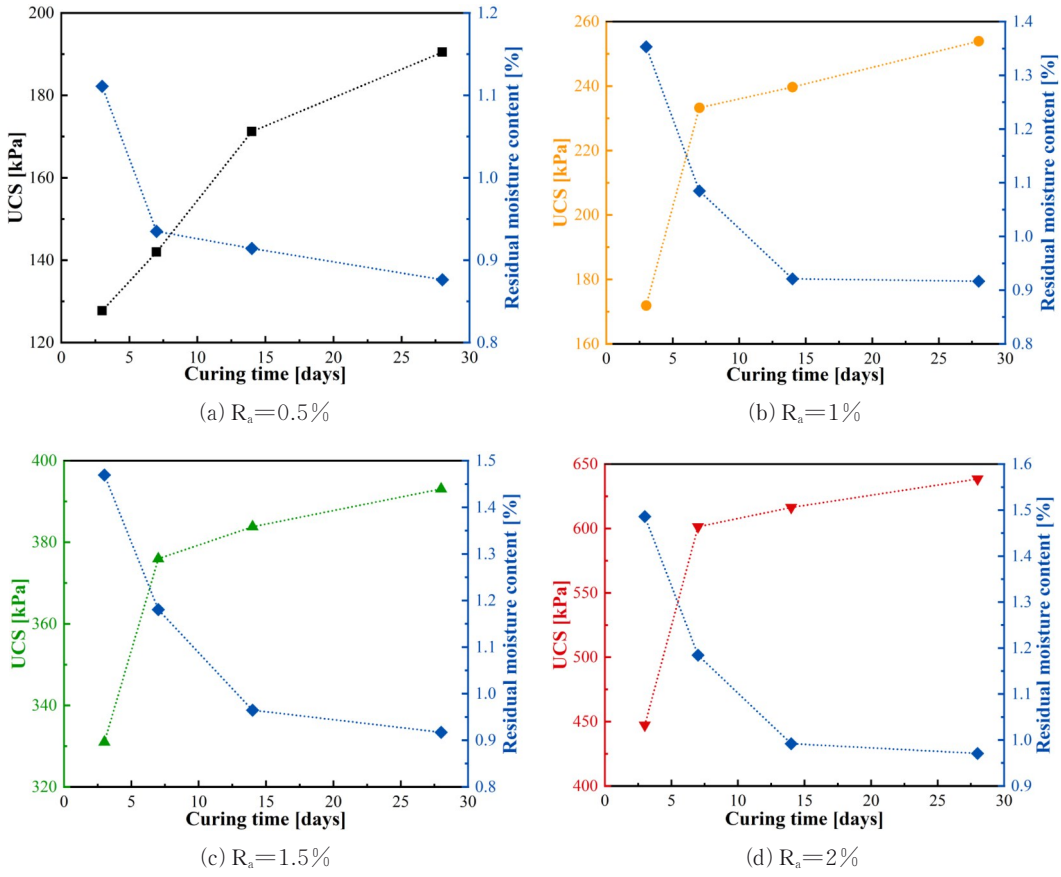


**Fig. 11 Relationship between UCS and residual moisture content of agar gum-treated sand at different curing times and concentrations**

relationship between residual moisture content and UCS. As shown in Fig. 12, as the moisture content decreases, the UCS of polymer-treated sand at various polymer concentrations increases significantly, reaching the highest compressive strength at the lowest moisture content. After curing, the gel between sand particles solidifies wrapping around sand particles in the form of envelopes, fibers, and films, which increase the cohesive forces between sand particles; treated sand soil begins to exhibit increased compressive strength, shear strength, and stiffness. To distinguish the contributions of moisture loss and gel structure evolution, we made a quantitative comparison for the 2% concentration specimens after 3 and 7 days of curing: UCS increased by 34.5% (from 447 kPa to 601 kPa), while residual moisture content decreased by 21.5% (from 1.49% to 1.17%). The strength gain was proportionally greater than the moisture reduction, indicating that the formation of interparticle bridges and a continuous gel network evolution was the dominant strengthening mechanism during this period. From 7 to 28 days, UCS increased by only 6.2% (from 601 kPa to 638 kPa), despite a continued moisture reduction of 17.1% (from 1.17% to 0.97%). This confirms that after the gel network matures, further moisture loss does not contribute significantly to strength improvement. Therefore, the strength increase is governed primarily by gel structure evolution in the early curing stage (0 – 7 d) and only secondarily by moisture loss in the later stage (7 – 28 d).

The relationship curves between the UCS of treated sand at various agar gum concentrations and

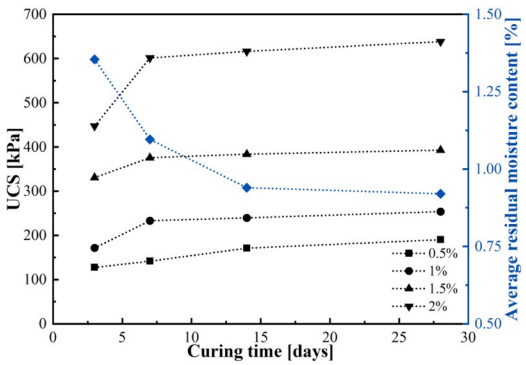


**Fig. 12 Relationship between UCS and average residual moisture content of samples at different curing times and concentrations**

the moisture content of the samples are shown in Fig. 13. At concentrations of 1%, 1.5%, and 2%, the UCS strength exhibits a significant negative correlation with the residual moisture content. This is likely since as moisture content increases, part of the agar gum between sand particles transforms into a sol state. The friction and bonding forces between sand particles and the sol-gel are weaker than those between sand particles and the dried solid agar gum, resulting in a decrease in the overall strength. Additionally, when the internal moisture content of the sample is high, water may exist in the form of free water between sand particles. When sand particles are subjected to force, this water acts as a lubricant; under pressure, the pore water pressure within the soil increases, leading to a decrease in overall strength.

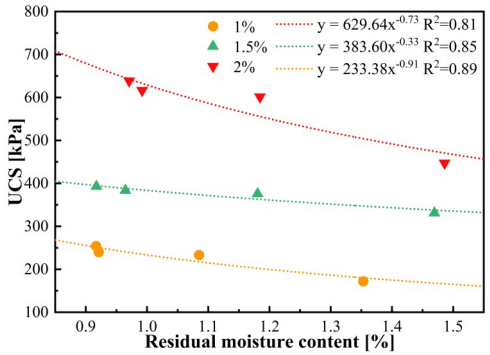


**Fig. 13　Relationship curves between the UCS and residual moisture content of agar gum-treated sand at different concentrations**

4.1.3　Effects of curing temperature

The stress-strain curves of 2% agar gum-treated sand at different curing temperatures are shown on Fig. 14. As can be seen in the figure, the stress-strain curves at different temperatures follow a similar pattern, but the peak strengths vary. Figure 15 shows the relationship between UCS and moisture content of 2% agar gum-treated sand at different curing temperatures. From this graph it can be concluded that, for the same concentration and curing time, the higher the curing temperature, the higher the UCS of the sample. Additionally, at the start of curing, the initial moisture content of all samples was the same. As the curing temperature changed, the residual moisture content of samples at different concentrations gradually decreased, and the UCS correspondingly increased.

The compressive strength data obtained from

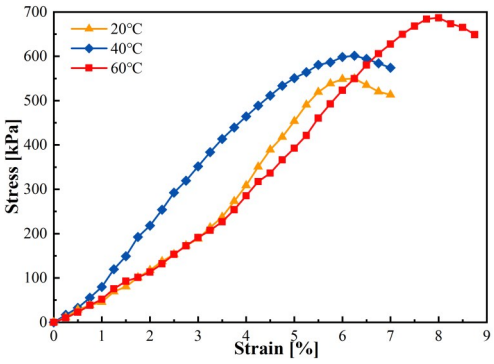


**Fig. 14　Axial stress-strain curves of 2% concentration agar gum-treated sand at different curing temperatures**

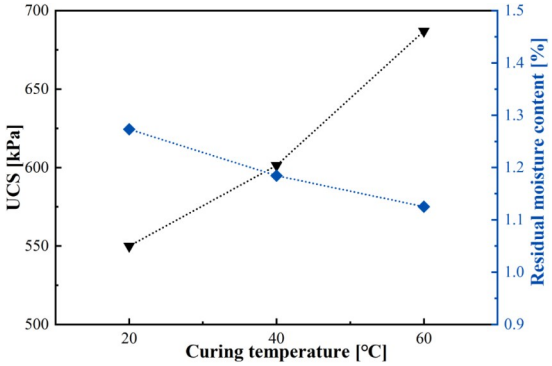


**Fig. 15　Relationship between UCS and residual moisture content of agar gum-treated sand at different curing temperatures**

the 2% agar gum concentration samples cured at 20 ℃ are in good agreement with the compressive strength-moisture content relationship curve obtained from samples cured at 40 ℃ (Fig. 13). However, the data obtained from samples cured at 60 ℃ do not align well with the other curves, possibly because the crystalline water present in the gel was unable to evaporate at high temperatures. As shown in Fig. 16, compressive strength shows a linear positive correlation with curing temperature of agar gum-treated sand. On average, the UCS increased by 11.78% for every 10 ℃ increase in temperature, and between 40 ℃ and 60 ℃, a 10 ℃ increase resulted in over 14% strength growth. However, the moisture content of samples cured at 60 ℃ for 7 days remained at 94.94% of that observed at 40 ℃, indicating that the overall change in residual moisture was not significant. This suggests that curing temperature affects sample strength through mechanisms beyond just moisture content.

4.1.4　Effects of curing conditions on failure pattern

Depending on the agar gum concentration and curing time, the failure modes of the specimens

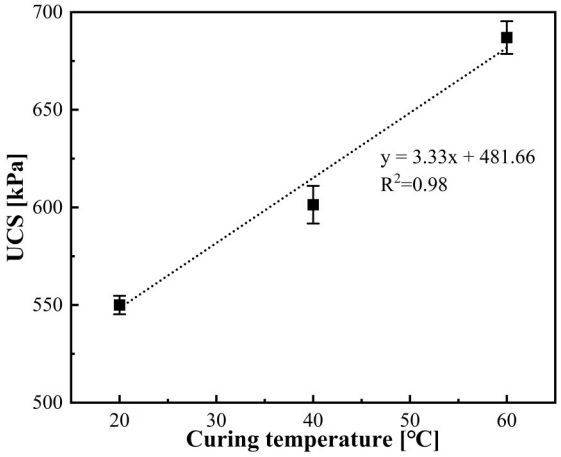


**Fig. 16 UCS of 2% concentration agar gum-treated sand at different curing temperatures**

vary. Six common typical fracture failure modes were selected for study. Figure 17(a) shows Y-type cracking failure, which is commonly observed in high-concentration (2%) samples after curing for7 days or more. Y-type failure involves the overall failure of the stress concentration point in the sample. After failure, the upper part of the sample forms a conical shape, with the conical cracking point located in the top region of the sample. The outer sand surface develops cracks in segments, ultimately fracturing into 2 - 4 parts. High-concentration specimens contain a larger quantity of agar gums uniformly distributed within the pores of the sand sample after adequate curing. Therefore, the gel-soil within the specimen achieves sufficient bonding and bridging during curing, resulting in higher overall strength. Additionally, such specimens have lower moisture content, and during failure, the sand fragments that split off are distinctly block-shaped, with the sand appearing dry and no visible moist areas. Such Y-shaped cracking is commonly observed in stronger samples, while weaker samples exhibit X-shaped cracking. In this context, stronger soils such as the highly cemented agar-soil samples, tend to fail in a brittle manner, with shear localizing along a single dominant failure plane inclined approximately 45 degrees to the loading axis. As loading continues past peak strength, the upper portion of the sample often shifts or rotates along this plane, resulting in a characteristic Y-shaped crack pattern that signifies sudden and localized failure.

In contrast, Fig. 17(b) illustrates an X-type failure, commonly observed in medium-concentration (1.5%) samples that have been adequately cured. This form of failure is characterized by an X-type crack initiating at the center of the sample. A conical cracking point develops at the center of the sample, with cracks propagating outward in block-like patterns, eventually causing the sample to fracture into 4 - 6 parts. Unlike the localized failure of Y-shaped cracks, X-shaped cracking reflects a more ductile failure mechanism, characterized by the formation of symmetrical shear planes on both sides of the sample. Although the agar gels fully during curing, the internal distribution of gel within the sand particles is less significant compared to that in higher-concentration samples, contributing to the nature of the failure.

Fig. 17(c) shows a sliding failure mode, commonly observed in high-concentration (2%) samples with a short-curing time (one day). This failure mode is typical of hard materials such as concrete or dry clay. The gelatinous clay within the specimen did not fully gel during curing, and the overall moisture content of the specimen was high. During failure, the sand blocks that split off were not clearly defined, and the central portion of the sand remained mostly moist. Figure 17(d) shows petal-type failure, which is commonly observed in samples with low concentration (1%) and short-curing time. After compression, the sample gradually develops tooth-like cracks, ultimately resulting in petal-type overall bulging. The gelatinous soil within the sample was fully bonded during curing, resulting in a high overall moisture content. During failure, the fragments separated from the sample were clearly visible, and the central part of the sample had a visible moist section. Figure 17(e) shows bottom crack failure, which is commonly observed in samples with low concentration (0.5%) and insufficient curing (less than 3 days). Under compression, the sample exhibited gradual swelling at the bottom, ultimately leading to failure due to development of bottom cracks. The overall moisture content of the specimen was low, and the clay soil inside did not fully gel during curing, causing uneven gel distribution. The bottom strength was lower than the overall strength of the specimen. Therefore, during compression failure, vertical cracks first develop at the weak bottom section, but the cracks propagate upward, and the specimen does not directly fracture.

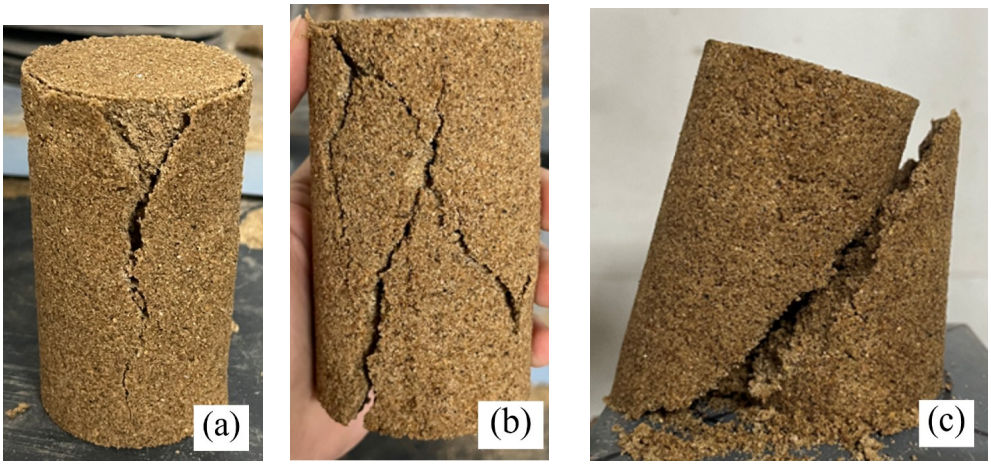


(a) Y-type failure　(b) X-type failure　(c) Sliding failure

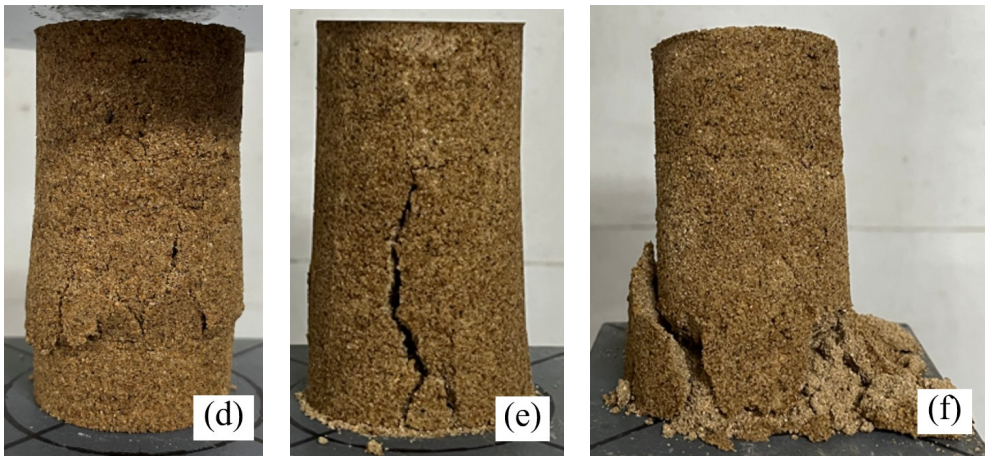


(d) Petal-type failure　(e) Bottom crack failure　(f) Bottom brittle failure

**Fig. 17　Failure patterns of agar gum-treated sand in UCS tests at different curing conditions**

Figure 17(f) shows brittle failure at the bottom, commonly observed in specimens with low concentration and adequate curing. During compression, no obvious crack development was observed on the outer side of the specimen. After reaching the strength limit, the bottom suddenly fractured. At this point, the overall moisture content of the specimen was very low, and there was no ductile failure. Therefore, the weak bottom region of the specimen underwent brittle failure.

When the specimens are fully cured for 28 days, agar gum-treated sand typically exhibits a Y-type failure. As the agar gum concentration decreases, the Y-type cracking point of the specimens gradually shifts downward, as shown on Fig. 18. During Y-type failure, the specimen fractures into two parts: the top conical section and the outer sand surface. The outer sand surface may fracture into 2 – 4 sections. The higher the agar gum concentration, the higher the position of the conical cracking point in the sample. At a 2% concentration, the cracking point is located at the top of the sample, and the volume of the top conical portion is smaller, as shown in Fig. 18(a). At this point, the volume of the top conical portion accounts for approximately 1/6 to 1/5 of the total sample volume. When the concentration is gradually reduced to 1.5%, the cracking point shifts from the top to the upper middle of the sample, and the volume of the top cone increases, accounting for approximately 1/4 to 1/3 of the sample volume, as shown in Fig. 18(b). The Y-type fracture pattern of the 1% concentration sample is shown in Fig. 18(c). At this point, the conical fracture point is located at the bottom of the sample, and after failure, the upper cone volume can account for approximately one-third to one-half of the total sample volume. It can be observed that as the concentration decreases, the volumes of the various parts of the fractured sample become increasingly similar, and the fracture point gradually shifts from the top to the bottom of the sam-

ple. The six failure modes, dominant failure controlling factor, critical threshold, and corresponding macro-mechanical response for each mode are summarized in Table 4.

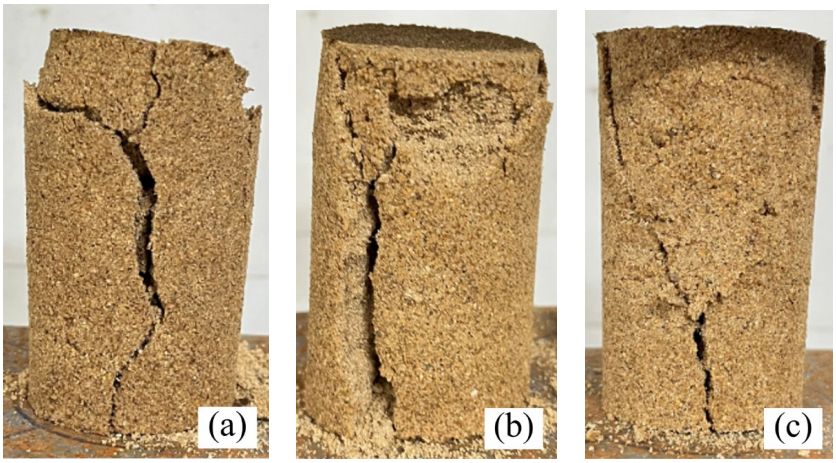


(a) $R_a$=2% (b) $R_a$=1.5% (c) $R_a$=1%

**Fig. 18 Distribution of Y-type cracking points in treated sand at various agar gum concentrations after 28 days of curing**

**Table 4 Summary of failure modes and their controlling factors with thresholds and responses**

| Failure mode | Dominant controlling factor | Critical threshold | Macro-mechanical response |
|---|---|---|---|
| Y-type (Fig. 17a) | Cementation uniformity (high) + low water content | Agar gum ≈2%, curing ≥7 days, residual moisture ≤1.2% | High peak strength, sharp post-peak drop, brittle failure |
| X-type (Fig. 17b) | Cementation uniformity (moderate) | Agar gum ≈1.5%, curing ≥7 days | Medium-high strength, symmetrical shear planes, moderate post-peak decline |
| Sliding (Fig. 17c) | High water content (lubrication) | Agar gum ≥1.5%, residual moisture > 1.5%, short curing (≤3 days) | Lower peak strength, gradual failure, no distinct cone |
| Petal-type (Fig. 17d) | Low concentration + moderate water | Agar gum ≈1%, curing 3 - 7 days | Low peak strength, bulging deformation, ductile-like response |
| Bottom crack (Fig. 17e) | Non-uniform cementation (weak bottom) | Agar gum ≤0.5%, curing ≤3 days | Very low strength, progressive cracking from bottom, no clear peak |
| Bottom brittle (Fig. 17f) | Low concentration + very low water | Agar gum ≤0.5%, curing ≥7 days, moisture <0.9% | Low strength, sudden brittle fracture at bottom, no warning |

### 4.2 Microstructural analysis

4.2.1 Effects of agar gum biopolymer concentration

Scanning electron microscope images of agar gum-treated sand cured at different concentrations for 7 days are shown on Fig. 19, with a magnification of 40x. At lower agar concentrations (0.5%), some of the sand is cemented, but the sample cross-section clearly shows areas where cementation is insufficient, resulting in numerous pores formed by particle detachment. At higher concentrations (1.5% and 2%), the specimen cross-section shows a higher strengthening effect, with agar gum uniformly distributed among sand particles. Figure 20 was obtained after binarizing SEM images; black represents non-porous areas and white represents pore areas. It is clear that as the concentration of the bonding solution increases, black areas increase and white areas decrease, indicating a reduction in the pores between soil particles. The pore contours in the binary image were retained as closed curves and displayed. The sum of the areas of all closed curves represents the pore area S1 in the sample cross-section. The ratio of pore area S1 to the total cross-sectional area S is the pore area ratio v of the sample cross-section. The local pore area ratios at various locations for samples of different concentrations are shown on Fig. 21. At lower agar concentration, the area of pore contours in the image is larger, indicating a higher pore area ratio of the sample cross-section. The pore area ratio v of the 0.5% sample can reach 19.94%. As agar gum concentration increases, the pore area ratio of the sample cross-section gradually decreases, dropping to 7.64% at 2% concentration. The higher the agar

gum content, the more polymer fills the pores between sand particles, and the more firmly the particles are bonded together. When preparing electron microscope samples, applying the same disturbance to the soil results in fewer particles detaching from the cross-section of samples with higher binder solution concentrations, leading to a reduction in cross-sectional pore area.

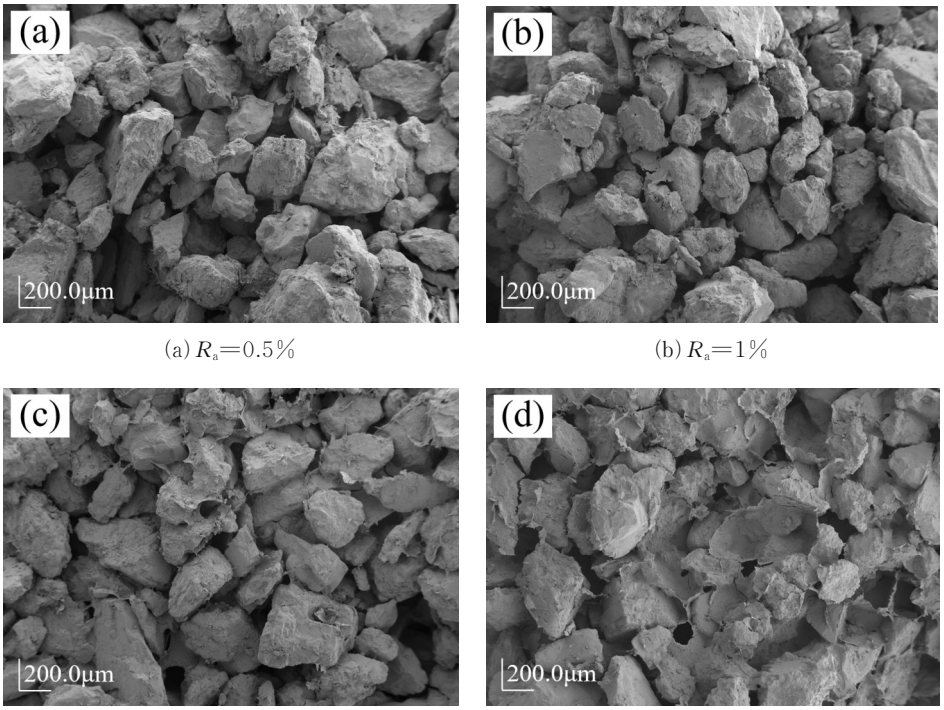


(a) $R_a$=0.5%　(b) $R_a$=1%

(c) $R_a$=1.5%　(d) $R_a$=2%

**Fig. 19　Scanning electron microscope images of cross-sections of agar gum-treated sand cured at different concentrations for 7 days (magnified 40 times)**

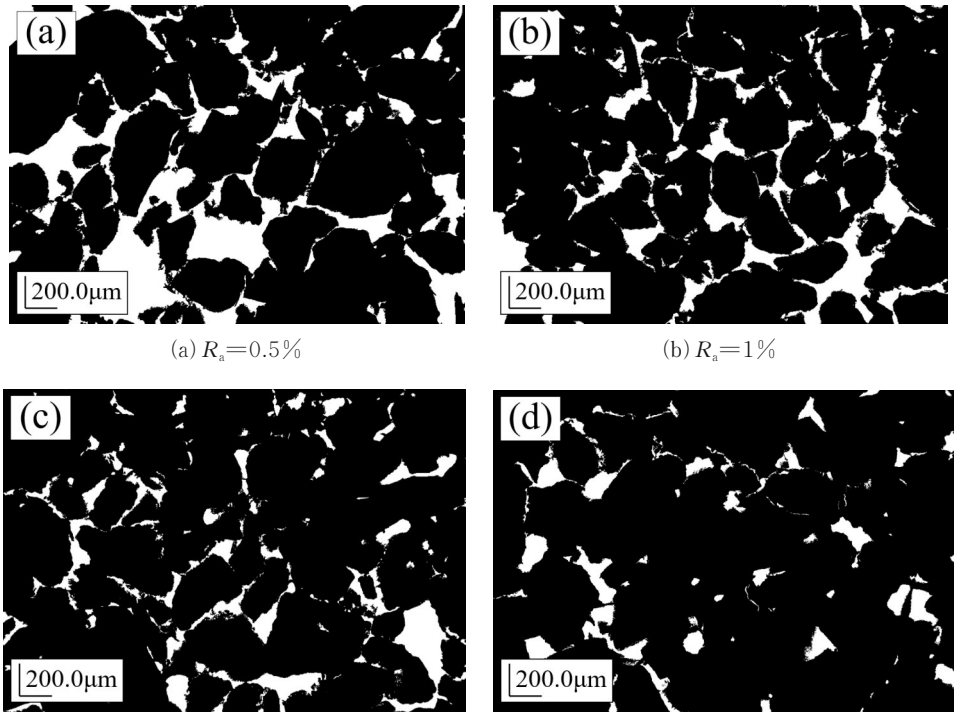


(a) $R_a$=0.5%　(b) $R_a$=1%

(c) $R_a$=1.5%　(d) $R_a$=2%

**Fig. 20　Binarized cross-sectional image of agar gum-treated sand cured for 7 days at different concentrations (magnified 40 times)**

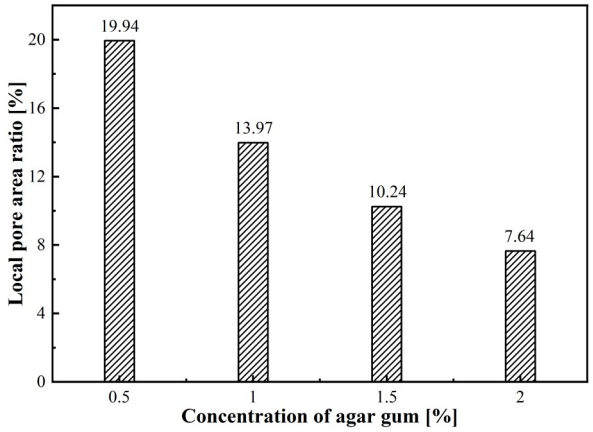


**Fig. 21 Local pore area ratio of agar gum-treated sand at various concentrations**

Observing the distribution morphology of agar gum at various concentrations, it can be noted that at lower concentrations, agar gum coats the surfaces of some sand particles, resulting in scattered bonding of the particles, whereas at higher concentrations, the gel can both coat the surfaces of sand particles and form bridges between them, thereby creating a uniform three-dimensional network structure. It can be inferred that when the agar gum concentration exceeds a certain threshold, the binder solution becomes oversaturated, resulting in excess gel filling the sand pores thereby reducing particle-to-particle contact. Therefore, there is an optimal concentration for polymer-reinforced sand.

4.2.2 Effects of curing time

Scanning electron microscope images of 2% agar gum-treated sand at different curing times are shown in Fig. 22, with a magnification of 40×. As can be seen in the images, the longer the curing time, the greater the degree of drying and shrinkage of the agar gum in the samples. At shorter curing times (3 days), most of the gel retains a relatively flat morphology, with a small portion exhibiting shrinkage, primarily distributed as a gel layer enveloping the surfaces of sand particles. During curing, water gradually evaporates and migrates from the gel, causing the gel matrix to shrink in volume, become thinner, and even curl. After 7 days of curing, most of the gel exhibits a dried and contracted state, with the gel matrix both enveloping the surfaces of sand particles and forming a relatively uniform network structure between particle pores, resulting in a more uniform distribution of the gel matrix. When the specimen is subjected to external forces, the dry gel between the particles provides a certain degree of strength and stiffness, thereby enhancing the overall strength of the specimen. As shown in Fig. 11(d), the effect of curing time on the compressive strength of the specimen follows a certain pattern: the strength of the 2% specimen after 7 days is 1.34 times that of the specimen after 3 days, while the strength of the specimen after 28 days is only 1.06 times that of the specimen after 7 days. As time progresses, the gel loses more water, leading to gradual increases in the specimen's shear strength, cohesion, and internal friction angle. When the specimen is sufficiently cured (around 7 days), the gel is distributed uniformly between particles, and the internal moisture gradually evaporates completely, resulting in the specimen achieving high strength and gradually stabilizing. In the later stages of curing, the evaporation rate of internal moisture slows down, the internal friction angle remains largely unchanged, and the increase in strength becomes increasingly smaller.

4.2.3 Effects of curing temperature

As shown in Fig. 23, the curing temperature exerts a pronounced effect on both the polymer gel volume and the final moisture distribution of samples after a curing of 1 day. At this early stage (1 day), the moisture content and the spatial distribution of dry and wet gels differ considerably among samples subjected to various temperatures. At room temperature (20 ℃) curing, the thermal gradient of the samples is lower, resulting in a smaller dehydration rate gradient. This allows internal moisture to continuously migrate towards the surface over a longer curing time, forming a more uniform moisture distribution. The cross-section contains a significant amount of undried gel. At 40 ℃, the overall moisture content of the samples decreases by 26.42%, and the undried gel of the cross-section becomes smaller. At 60 ℃, the moisture content of the sample decreases significantly by 61.01%. The sample dehydrates more rapidly and over a larger area, thereby quickly forming a dry gel portion with lower permeability and higher stiffness, which hinders further reduction in the moisture content of the undried gel portion at the center.

Scanning electron microscope images of 2% agar gum-treated sand cured at different temperatures

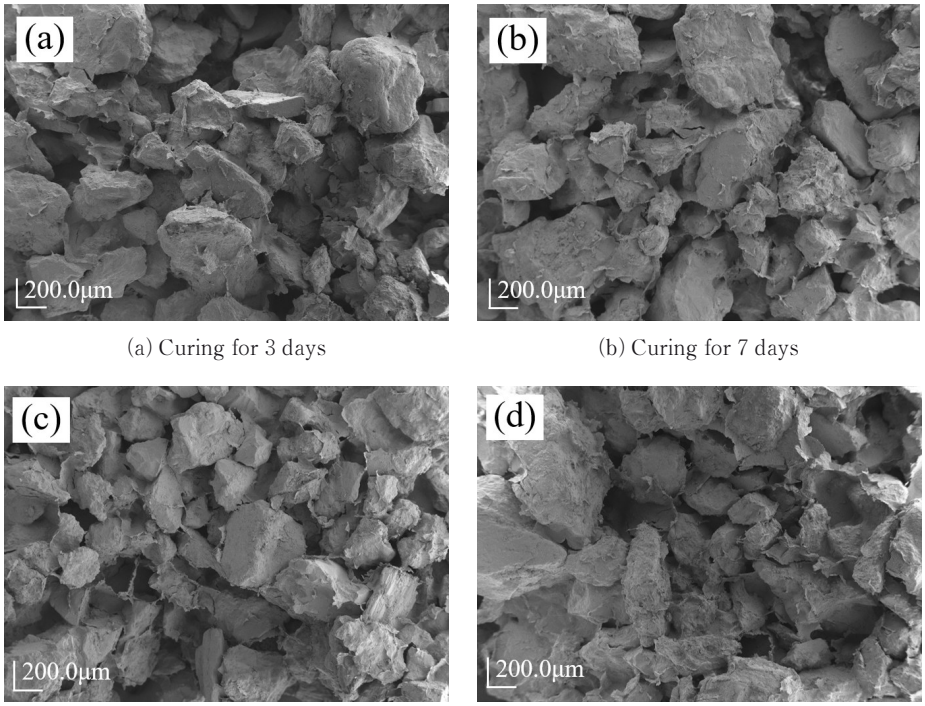


(a) Curing for 3 days　　(b) Curing for 7 days

(c) Curing for 14 days　　(d) Curing for 28 days

**Fig. 22　Scanning electron microscope images of cross-sections of agar gum-treated sand with 2% agar gum at different curing times (magnified 40 times)**

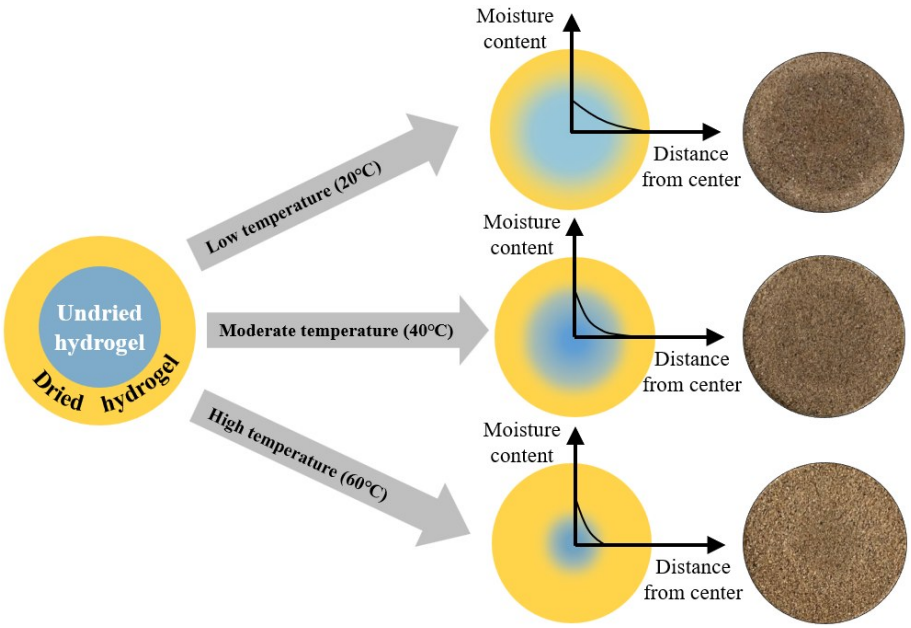


**Fig. 23　Schematic diagram of the volume and water distribution of polymer hydrogel in the cross-section of samples at different curing temperatures after a curing of 1 day**

for 7 days are shown on Fig. 24. From SEM images magnified 70 times, it can be observed that the morphology and distribution of the agar gum vary significantly with temperature. At 20 ℃, the agar gum appears as thin films or strips attached to the surfaces of sand particles or distributed between them, as shown in Fig. 24(a). At 40 ℃, the gel matrix rapidly forms a medium-thickness outer shell, inhibiting further contraction of the gel body due to its low permeability and high stiffness. At this temperature, the agar gum appears as thicker, smaller-area strip-like or sheet-like thick films, adhering to the surfaces of sand grains or between sand grains, with irregular shapes, as shown in Fig. 24(b). When the temperature reaches 60 ℃, the rate of water exchange between the gel and air increases significantly, leading

to the rapid formation of a hard outer shell. Compared to the intermediate temperature condition, the gel matrix undergoes a significant contraction, and some membrane-like gels develop cracks. The gel takes on a more complex, fragmented form, with small pieces distributed between sand particles, bonding them together, as shown in Fig. 24(c). The gel shows the least shrinkage at moderate temperatures (40 ℃), with its outer shell forming in a relatively short time. At higher curing temperatures, the thicker hydrogel outer shell exhibits the highest strength.


(a) 20 ℃ (b) 40 ℃ (c) 60 ℃

**Fig. 24 Scanning electron microscope images of 2% agar gum-treated sand cured at different temperatures for 7 days.**

## 5 Mechanism

The fundamental reason for the change in the macroscopic physical and mechanical properties of sand under external loads lies in the alteration of its microstructure. When agar gum polymer solution is mixed with sand, it coats the surfaces of sand particles, fills the pores between particles, and effectively binds the particles together, thereby improving the mechanical properties of the sand. Sand particles are connected by polymer bridges with strip-like or membrane-like structures, and the pores between sand particles are also filled with polymers. After analyzing many SEM images, it can be concluded that the relationship between polymers and sand particles involves three mechanisms: surface coating of particles, pore filling, and inter-particle connection, as shown in Fig. 25. The schematic diagram of the agar gum development process is shown on Fig. 26. During the initial curing stage, the gel encapsulates sand particles and fills the sand pores (Fig. 26a). In the early stage, the outer layer of the agar gum gradually dehydrates to form a gel shell, which possesses hardness and cohesive force, imparting a certain strength to the sample (Fig. 26b). During the curing process, the gel gradually dehydrates and contracts, causing the outer shell to thicken. Ultimately, it exhibits the three distribution states of sand particle coating, pore filling, and inter-particle bridging. At this stage, the agar gum is fully cured and has good bonding with the sand particles, forming a relatively stable three-dimensional network structure (Fig. 26c).

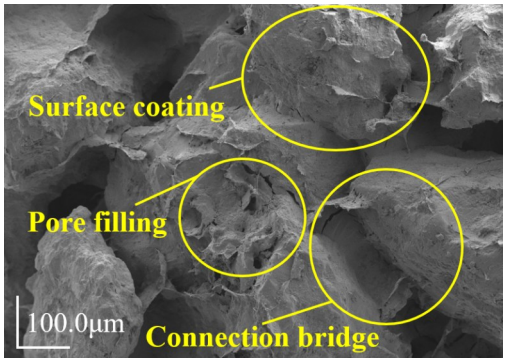


(a) SEM diagram

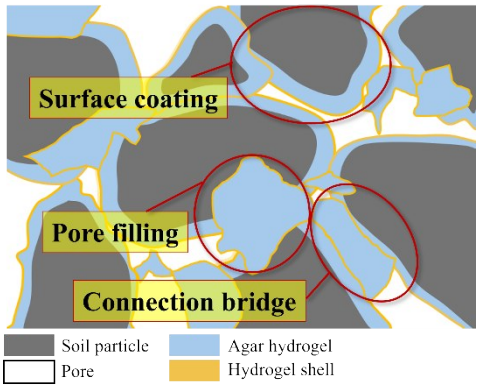


(b) Colorings diagram

**Fig. 25 The distribution of polymer gel in sand particles**

### 5.1 Effects of agar gum biopolymer concentration

Agar gum concentration modifies the macroscopic mechanical behavior of sand by regulating the mor-

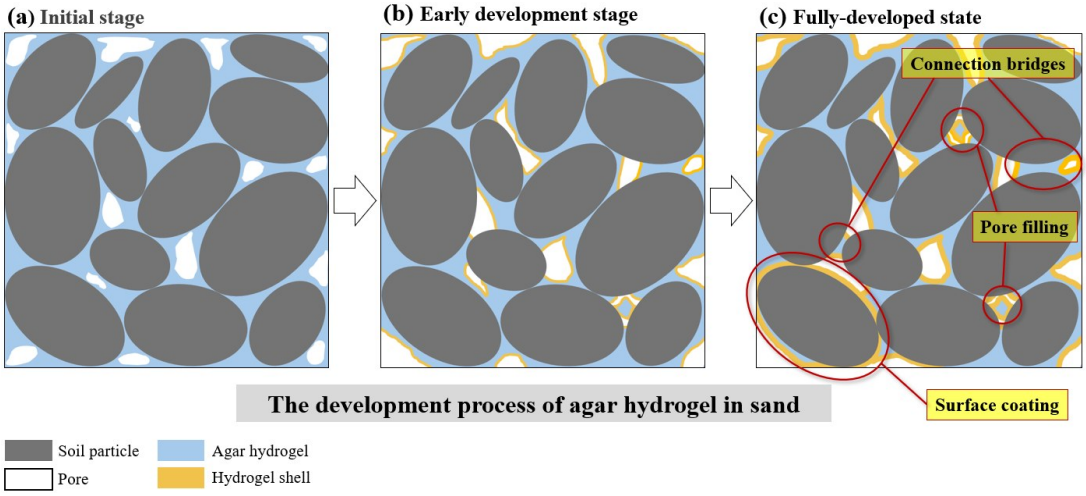


**Fig. 26　The development process of agar gum hydrogel in sand**

phology of the gel network and pore structure. At low agar gum concentrations (0.5%), the gel exhibits a scattered distribution, resulting in widespread areas of insufficient gelation. Microscopically, this manifests as localized point-wise gelation (Fig. 19a), while macroscopically, it corresponds to significant dispersion in the stress-strain curve (Fig. 8a). This state only confers cohesive strength to the sand foundation, with a UCS of approximately 127.69 kPa at a 3-day curing time. When the concentration increases to 1%, the gel forms an initial local connection network between sand particles, and the stress-strain curve exhibits consistent strain softening characteristics (Fig. 8b). The failure strain also increases systematically with the increase in concentration: at a 7-day curing time, strain is approximately 4% at a 0.5% concentration (Fig. 8a) and reaches 6.2% at a 2% concentration (Fig. 8d). This indicates that a higher gel content leads to a greater deformation before fracture, which may be due to the denser gel network having a stronger energy dissipation capacity.

When the concentration reaches the critical threshold of 1.5% - 2%, the agar gum forms a three-dimensional network structure (Fig. 19c - d), causing particle wrapping and bridging. At this point, the macroscopic mechanical behavior shows a typical strain softening curve with a gentle post-peak segment (Fig. 8c - d), indicating that the gel network suppresses brittle failure through an energy dissipation mechanism, conferring quasi-ductile properties to the material. Quantitative analysis of the microporous structure further supports this mechanism: binarized images show that the pore area ratio v of the sample cross-section decreases systematically as the concentration increases from 0.5% to 2% (Fig. 20～22). This phenomenon is attributed to insufficient gel coverage at low concentrations causing particle detachment, resulting in a high porosity of 19.94%; whereas at medium to high concentrations, the gel fully fills the pores and bridges the particles, reducing the porosity to 7% - 12%. The reduction in porosity not only enhances the overall density of the treated sample but also significantly increases interfacial adhesion by increasing the effective bonding area, enabling the 2% concentration sample to achieve a 28-day strength of 638.47 kPa (3.35 times that of the 0.5% sample).

As the bonding solution concentration increases, the strength growth pattern of the sample exhibits a non-linear characteristic. In the low concentration range (0.5% - 1%), a 100% increase in concentration only results in a strength increase of 0.33-0.34 times, whereas in the high concentration range (1.5% - 2%), the same concentration increase leads to a strength increase of 0.6-0.62 times, confirming the enhancing effect of the continuous network on load transfer. At low concentrations, the polymer primarily fills the pores between particles, resulting in limited enhancement of shear strength. With further increase in agar content, the polymer encapsulates the sand particles, thereby further increasing the sample strength. Notably, specimens at a 2% concentration reached 90% of the 28-day strength at 7-day curing, indicating that high-concentration can accelerate the maturation of the cementing network, which has significant practical application value in en-

gineering.

Scanning electron microscopy observations also revealed the potential risks of concentration overload: when the concentration exceeds 2%, excess gel forms thick gel films between particles, which although further reduces porosity, may weaken the mechanical interlocking effect between sand particles. This phenomenon suggests the existence of an optimal concentration threshold. Combining the strength growth rate inflection point (the largest increase occurs in the 1.5% - 2% range) with microstructural characteristics, it is recommended that engineering applications use the 1.5% - 2% range as the optimal concentration window.

### 5.2 Effects of curing time

The development of the mechanical properties of agar gum-treated sand is primarily influenced by the evolution of moisture content and the gel phase transition process during the curing time. As shown in Fig. 11, as the curing time increases, the residual moisture content of samples at various concentrations systematically decreases, while the UCS correspondingly increases. This phenomenon is attributed to the continuous evaporation of water, which triggers a physical phase transition in the gel. The loss of free water promotes the gradual transformation of the initial sol-gel state of agar gum into a solid gel matrix, thereby enhancing the cohesive force between sand particles and the interfacial adhesive strength. After 14 days of curing, both strength and moisture content changes stabilize (Fig. 11c-d), indicating that the gel network has entered a mature stage.

Samples with different concentrations exhibit significant differences in water retention characteristics. Under the same curing time conditions, the residual moisture content of samples with concentrations between 1.5% and 2% is consistently higher than that of low-concentration samples (Fig. 11a-d). For example, at 3 days of curing time, the moisture content of the 2% sample is 1.34 times that of the 0.5% sample. This phenomenon is attributed to the three-dimensional network structure formed by high-concentration agar gum, which effectively binds bound water and slows down the internal water migration rate. However, long-term curing weakens the influence of concentration gradients, and by the 28-day curing time, the water content ratio decreases to 1.11 times (Fig. 12), reflecting that the water diffusion process ultimately tends toward homogenization.

The contribution of curing time to strength development exhibits a non-linear characteristic. Low-concentration samples showed a strength increase of 11.2% between 14 and 28 days (Fig. 11a), revealing their slow-maturing binder network characteristics; in contrast, high-concentration samples exhibited an increase of only 2% - 3.6% during the same period (Fig. 11c - d), confirming their early rapid curing advantage. Notably, the 2% concentration sample achieved 94.19% of the 28-day strength at the 7-day curing time (Fig. 11d), providing a theoretical basis for engineering applications to shorten the curing cycle.

Scanning electron microscope images (Fig. 22) provide direct evidence for the microscopic mechanisms. In short-curing time samples, the gel forms a smooth coating layer on the surface of sand particles (Fig. 22a), retaining sol characteristics; as curing progresses, water evaporation causes the gel to contract and curl, forming interparticle bridges (Fig. 22b); while long-term specimens develop a uniform gel network structure (Fig. 22c-d), forming a three-dimensional network system between sand particles and gel. By the 7-day curing time, the gel network is largely formed (Fig. 22b), corresponding to the strength entering a plateau phase (Fig. 12). Further extending the curing time causes the gel to undergo minor contraction and densification, contributing little to strength enhancement. The microscopic evolution is highly consistent with macroscopic strength growth.

It is evident that the curing process of treated sand has a critical threshold. The 7-day period represents the gel network formation stage, during which gel morphology transitions from smooth, sheet-like coatings (Fig. 22a) to a shrunken, bridged network (Fig. 22b), driven by rapid water evaporation. For the 2% concentration specimens, UCS increases by 34.5% (from 447 to 601 kPa) between 3 and 7 days, while residual moisture decreases by 21.5% (from 1.49% to 1.17%). This strength gain exceeds the rate of moisture loss, confirming that gel structure

evolution dominates this stage and contributes over 90% of the total strength growth (Fig. 11d). After 7 days, the system enters the bonding stabilization phase (Fig. 22c-d), where residual water slowly desorbs, resulting in only minor strengthening. From 7 to 28 days, UCS increases by only 6.2% (from 601 to 638 kPa) despite a continued moisture reduction of 17.1% (from 1.17% to 0.97%), further demonstrating that once the gel network matures, additional drying has a limited effect on strength enhancement. This two-stage mechanism originates from a fundamental shift in water migration: free water rapidly dissipates in the early stage to form the bonding framework, whereas bound water desorption only slightly adjusts structural density in the later stage. High-concentration agar gum achieves early strength enhancement through a dense network (Fig. 11d), while low-concentration systems rely on progressive strengthening via discrete gelation points (Fig. 11a). The 7-day curing time thus serves as the critical node for gelation maturity (Fig. 12), establishing a scientific benchmark for optimizing engineering curing cycles.

### 5.3 Effects of curing temperature

Curing temperature regulates the mechanical properties of agar gum-treated sand through a dual pathway. When the temperature rises from 20 ℃ to 60 ℃, the UCS of the 2% concentration sample shows a significant increase of 25%. This strengthening effect is primarily attributed to the accelerated water migration caused by temperature, as higher temperatures systematically reduce the residual moisture content (Fig. 15), driving the transformation of the sol-state agar gum into a solid gel matrix. However, it is worth noting that the strength increase of the 60 ℃ sample far exceeds its moisture content decrease, and its data points significantly deviate from the moisture content-strength fitting curve (Fig. 13), indicating the presence of a strengthening mechanism independent of moisture content.

Changes in curing temperature also induce uneven moisture distribution. Fig. 27 illustrates the effect of curing temperature on agar gum. At room temperature (20 ℃), the dehydration rate of the agar gum is gradual, with water uniformly diffusing to form a continuous film, resulting in a thin outer hard shell (Fig. 27a). Under moderate temperature conditions (40 ℃), moderate dehydration forms a medium-thickness outer shell, whose low permeability effectively inhibits internal shrinkage, preserving a larger gel volume (Fig. 27b). Under high-temperature conditions (60 ℃), the gel surface hardens rapidly, causing the outer shell to form quickly, with more pronounced shrinkage of the gel matrix (Fig. 27c). Cracks may appear in some parts of the internal film (Fig. 27d), leading to obstructed water migration within the sample and the formation of a "dry exterior and wet interior" dual-layer structure, exacerbating uneven gelation. Specimens cured at 40 ℃ achieve the optimal balance between bonding uniformity and network density (Fig. 24b), with moderate bonding shell thickness and no significant cracks.

Scanning electron microscope images reveal the reconstructive effect of temperature on the morphology of the gel (Fig. 24). Under 20 ℃ curing conditions, the gel exhibits a thin and flat film morphology, with molecules maintaining an ordered helical structure, forming a homogeneous gel layer with limited mechanical performance. At a curing temperature of 40 ℃, the molecular conformation undergoes an entropy-driven transformation. This coil-to-helix transition is well documented for agar gum and is known to promote the formation of additional junction zones, thereby increasing cross-linking density[34]. Disordered curled polymer chains promote molecular cross-linking, constructing a strong and tough three-dimensional network. When the temperature increases to 60 ℃, the gel fractures into complex small pieces due to excessive shrinkage. Although this enhances local bonding strength, microscopic cracks exacerbate structural heterogeneity, potentially leading to overall strength reduction. The importance of this conformation transition lies in high temperatures disrupting molecular order and promoting interchain cross-linking, while the cooling process permanently solidifies the cross-linked structure, ultimately imparting a denser gel network to the high temperature cured samples. Additionally, higher temperatures mean more frequent interpenetration between the gel and sand particles before complete solidification, resulting in stronger bridging and network structures, which reasonably explains the high-

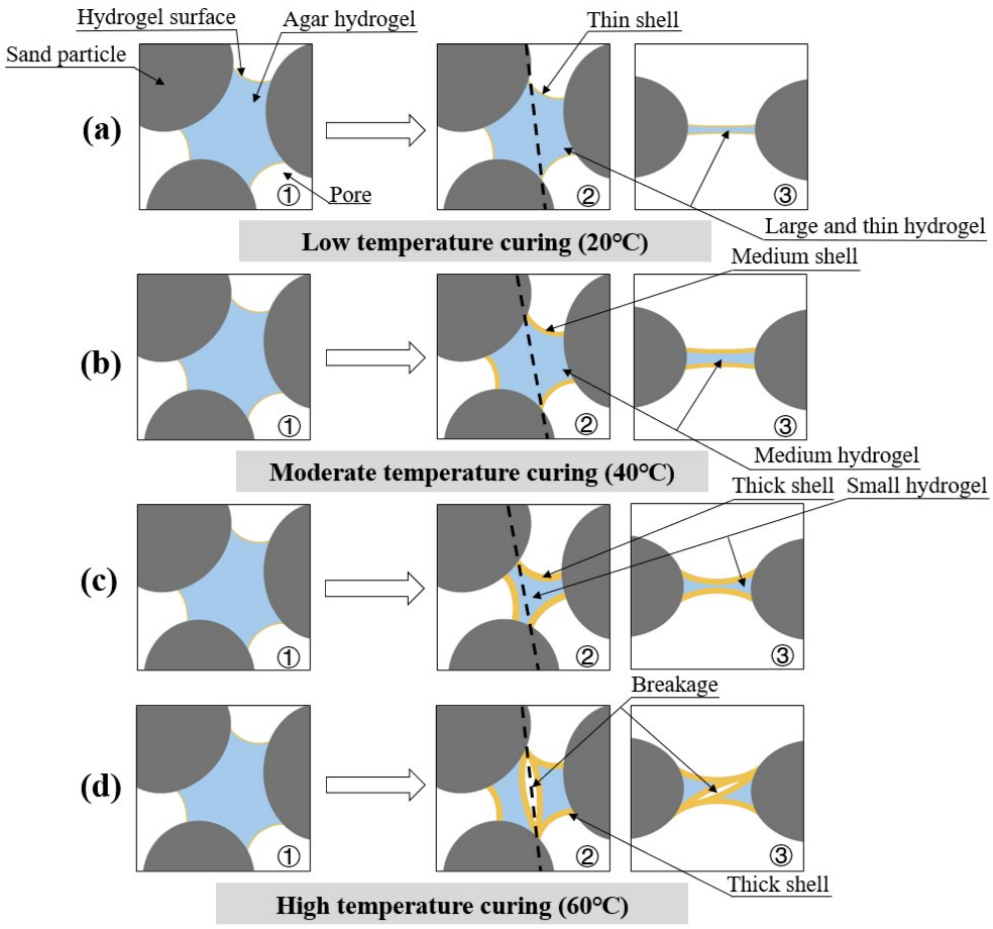


Note: (a) cured at 20 ℃, (b) cured at 40 ℃, (c) cured at 60 ℃, gel shrinkage, (d) cured at 60 ℃, gel cracking

**Fig. 27 Schematic diagram of the effect of curing temperature on agar gum**

est slope of strength increase in the 40 ℃ - 60 ℃ range shown in Fig. 15. Linking gel morphology The macro-mechanical effect of gel network morphology in terms of UCS strength is as follows: at 20 ℃, thin flat films (Fig. 24a) yield a UCS of 549 kPa; at 40 ℃, thicker strip-like gels (Fig. 24b) increase the UCS to 627 kPa (an increase of 14.3%); at 60 ℃, fragmented and cracked gels (Fig. 24c) produce the highest UCS of 687 kPa (an increase of 9.5% relative to 40 ℃). The strengthening from 40 ℃ to 60 ℃ exceeds that could be expected from moisture loss alone (residual moisture decreased by only 5.1%), suggesting that molecular conformation change and the resulting fragmented gel morphology provide additional strengthening beyond dehydration.

We can conclude that curing temperature enhances sand strength through a synergistic mechanism —both reducing moisture content and optimizing the gel network restructuring. The 40 ℃ - 60 ℃ temperature range provides the optimal balance between gel uniformity and cross-linking density, while temperatures above 60 ℃ carry the risk of structural heterogeneity. Temperature, along with agar concentration and curing time, form a three-dimensional system for performance regulation, with a 40 ℃ - 60 ℃ curing temperature window balancing efficiency and stability.

### 5.4 Destruction mechanism

The interaction between agar gum concentration and curing time discussed in Section 4.1.4, determines the formation of six typical failure modes (Fig. 17) which result from the interaction between the gel network state and the moisture content. When the specimen is subjected to external loads, the sand-gel mixture forms an integrated load-bearing system. Within this system, the movement of sand particles is restricted, and particle movement shifts from high-stress chain zones to low-stress chain zones. As the microstructure becomes unstable, stress concentration causes sand particles to undergo compression, tension, and rotation. When particle movement exceeds the polymer membrane′s load-bearing limit, inter-particle failure occurs at the weakest points of the polymer membrane bond. The

underlying mechanisms of this failure can be summarized as follows:

In samples with high agar concentration (≥2%) and long-curing time (≥7 days), agar gum forms a cross-linked, continuous, dense network, which shows a mechanical behavior similar to sandstone-like rocks. Microscopically, this manifests as the bonding phase uniformly covering the particle surfaces, while macroscopically, it results in efficient stress transmission along the axial direction, leading to significant tensile stress concentration at the top of the sample, ultimately triggering a Y-type cracking pattern (Fig. 17a). Notably, the uniformity of cementation decreases with decreasing concentration: when the concentration drops to 1.5%, the formation of local cementation islands causes stress concentration points to migrate to the middle and upper parts (Fig. 18b); when the concentration further decreases to 1%, the cementation gradient distribution causes the cracking points to settle at the bottom of the specimen (Fig. 18c). When the concentration decreases to the critical value of 0.5%, the synergistic effect of point-like bonding and gravitational settling forms a weak zone at the bottom, becoming the trigger for bottom bulging or brittle failure (Fig. 17e-f).

Water content, as a key parameter characterizing the curing process, regulates the transition of failure modes by altering the rheological properties of the gel. High water content primarily occurs in short-curing time specimens (e. g., 2%-1d combination), where unlinked gel exerts a lubricating effect, significantly reducing interparticle friction resistance and inducing overall shear slippage akin to saturated clay (sliding failure in Fig. 17c). Moderate water content is observed in low-concentration, short-curing time specimens (1%-1d), where the failure mechanism involves the coupling of gel chain stretching and fracture with the rearrangement of unbound sand particles, ultimately forming a petal-shaped morphology (Fig. 17d). Extremely low water content in long-term cured specimens induces a brittle transformation of the entire specimen. High-concentration systems exhibit brittle fracture characteristics (Y/X-type failure), while low-concentration systems experience fragmentation and collapse due to point-like cementation hardening (Fig. 17f).

The failure behavior results from the selection of pathways for energy release within the material, a process directly regulated by the spatial configuration of the cementation network. In uniformly strongly cemented systems (high concentration, long-term curing), stress concentrates along the axial height, ultimately releasing energy through conical cracks in a single event, manifesting as Y-type cracking with the conical volume accounting for only 1/6 to 1/5 of the total (Fig. 18a). In non-uniform cementation systems (low concentration), gravitational settling forms a weak cementation layer at the bottom, and stored energy is preferentially released along this weak zone, leading to progressive swelling or sudden brittle fracture (Fig. 17e-f). In systems with weak local surfaces (medium concentration and long-curing time), non-uniform regions in the network cementation induce multi-directional crack intersection and expansion, forming typical X-type through cracks (Fig. 17b).

In uniformly strong cemented systems, 28-day long-term samples generally exhibit Y-type cracking (Fig. 18), with the cracking points continuously shifting downward as concentration decreases. This confirms the controlling effect of cementing uniformity on failure pathways. This entails a warning for long-term engineering projects: to prevent the risk of brittle collapse at the bottom, high-concentration structures should be designed as brittle materials to avoid cone failure.

## 6 Conclusion

The aim of this study was to investigate the effects of polymer concentration, curing time, and curing temperature on the UCS of agar gum-treated sand and the underlying mechanisms leading to UCS changes. The following key findings were obtained from analysis of experimental data and specimen failure patterns.

1) Effect of agar gum concentration: The UCS increased with increasing agar concentration due to the formation of a three-dimensional gel network, and pore filling. At 2% concentration, the 28-day UCS reached 638.5 kPa, which is 3.35 times that at 0.5%. The failure strain increased from ~1.7% to ~3.2% as concentration rose from 0.5% to 2%,

indicating that deformation capacity increased with higher gel network density. From an engineering perspective, although agar gum (1.5% - 2% dosage) has a higher material cost (≈120 - 160 RMB/ton) than cement stabilization (≈25 RMB/ton at 5% dosage), its environmental benefits (no $CO^2$ emission, no soil pH rise, biodegradability) make it a better choice for ecologically sensitive or temporary applications.

2) Effect of curing time and residual moisture: Seven days of curing was found to be the critical threshold for gel network maturation, achieving > 90% of the 28-day strength. The UCS was negatively correlated with residual moisture content; the probable cause is that free water lubricates particle contacts while solid gel provides bonding.

3) Effect of curing temperature: The UCS increased with temperature, with an average gain of 11.78% per 10 ℃ rise. The 40 ℃ - 60 ℃ range induced molecular conformation changes that increased cross-linking density, but temperatures above 60 ℃ might have caused excessive gel shrinkage and microcracks. For field application, 40 ℃ - 60 ℃ curing can be achieved during summer, or using solar greenhouse covers (raising temperature by 15 ℃ - 25 ℃), or industrial waste heat. Challenges include temperature uniformity and moisture control, which require attention in pilot-scale trials.

4) Failure modes and microscopic mechanisms: Six failure modes (Y-type, X-type, sliding, petal-type, bottom crack, bottom brittle) were identified, controlled by gel uniformity and moisture distribution. High concentration (≥1.5%) and long curing time (≥7 d) were found to cause brittle Y/X-type failure; low concentration (≤1%) and short curing (≤3 d) caused progressive or swelling failure. Microscopic strengthening arose from particle coating, pore filling, and interparticle bridging by the hardened gel.

5) In engineering applications, a combination of agar gum concentration of 1.5% - 2.0%, curing time of 7 days, and curing temperature of 40 ℃ - 60 ℃ is recommended for sand strengthening. This combination balances strength efficiency and structural uniformity while avoiding risks of interface weakening and structural heterogeneity.

The present study has some limitations due to time constraints. Quantitative analysis of stress concentration, crack propagation, and energy release mechanisms for the six failure modes were not included. These aspects will be addressed in future numerical simulations (DEM/FEM). Moreover, we will further explore the mechanical theory behind the experimental data by adopting appropriate constitutive models for soils (e. g. , elastoplastic or damage models) to better explain the observed stress-strain behavior and failure mechanisms. Future research will also conduct dynamic triaxial tests to investigate liquefaction resistance and explore long-term durability under dry-wet and freeze-thaw cycles.

## References

[1] Liu J, Feng Q, Wang Y, et al. Experimental study on unconfined compressive strength of organic polymer reinforced sand[J]. International Journal of Polymer Science, 2018, 2018: 3503415.

[2] Rezaeimalek S, Huang J, Bin-Shafique S. Evaluation of curing method and mix design of a moisture activated polymer for sand stabilization[J]. Construction and Building Materials, 2017, 146: 210-220.

[3] Feng Q, Liu J, Lu Y, et al. Experimental study on strength of sand reinforced with composite reinforcement agent[J]. Journal of Engineering Geology, 2017, 25(4): 903-911.

[4] Zhang H D, Li H F, Li H Y, et al. Experimental study on strength characteristics of palm fiber-reinforced soil [J]. Mineral Exploration, 2021, 12(5): 1264-1271.

[5] Zhou L L, Su L, Ling X Z, et al. Experimental and numerical modeling on liquefaction resistance of fiber reinforced sand [J]. Journal of Engineering Geology, 2021, 29(5): 1567-1576.

[6] Zhu H H, Gao Y X, Li Y H, et al. Experimental study of pullout behavior of horizontal anchor plates in geogrid reinforced sand[J]. Rock and Soil Mechanics, 2022, 43 (5): 1207-1214.

[7] Cheng G, Wang S J, Li X, et al. Experimental study on bio-cemented solidification fiber-reinforced sandy clayey purple soil[J]. Chinese Journal of Underground Space and Engineering, 2021, 17(6): 1829-1838.

[8] Zhou G Y, Pan K, Yang Z X. Energy-based assessment of cyclic liquefaction behavior of clean and silty sand under sustained initial stress conditions[J]. Soil Dynamics and Earthquake Engineering, 2023, 164: 107609.

[9] Fan H H, Gao J E, Wu P T. Prospect of researches on soil stabilizer[J]. Journal of Northwest Sci-Tech Univer-

sity of Agriculture and Forestry (Natural Science Edition), 2006, 34(2): 141-146, 152.

[10] Zhou H L, Shen X D. Application research situation and prospect of soil stabilizer[J]. Materials Review, 2014, 28(9): 134-138.

[11] Rashid A S A, Latifi N, Meehan C L, et al. Sustainable improvement of tropical residual soil using an environmentally friendly additive[J]. Geotechnical and Geological Engineering, 2017, 35(6): 2613-2623.

[12] Worrell E, Price L, Martin N, et al. Carbon dioxide emissions from the global cement industry[J]. Annual Review of Energy and the Environment, 2001, 26: 303-329.

[13] Taylor H F W. Cement Chemistry[M]. 2nd ed. London: Thomas Telford, 1997.

[14] Liu S, Luo G H, Zhang J Q, et al. The reinforcement effect of new polyurethane materials to sandy soil and its environmental effect[J]. Journal of Hubei Polytechnic University, 2021, 37(3): 10-13.

[15] Zhang C Y, Yu Y X, Min W, et al. Experimental study on direct shear test of sand reinforced by water-soluble polymer[J]. Journal of Hebei University of Engineering (Natural Science Edition), 2021, 38(3): 13-21.

[16] Smitha S, Sachan A. Use of agar biopolymer to improve the shear strength behavior of Sabarmati sand[J]. International Journal of Geotechnical Engineering, 2016, 10(4): 387-400.

[17] Zhang L N. Natural Polymer Science and Materials[M]. Beijing: Chinese Science Press, 2007.

[18] Chang I, Im J, Lee S W, et al. Strength durability of gellan gum biopolymer-treated Korean sand with cyclic wetting and drying[J]. Construction and Building Materials, 2017, 143: 210-221.

[19] Chang I, Im J, Prasidhi A K, et al. Effects of xanthan gum biopolymer on soil strengthening[J]. Construction and Building Materials, 2015, 74: 65-72.

[20] Qureshi M U, Chang I, Al-Sadarani K. Strength and durability characteristics of biopolymer-treated desert sand[J]. Geomechanics and Engineering, 2017, 12(5): 785-801.

[21] Muguda S, Booth S J, Hughes P N, et al. Mechanical properties of biopolymer-stabilised soil-based construction materials[J]. Géotechnique Letters, 2017, 7(4): 309-314.

[22] Chang I, Lee M, Tran A T P, et al. Review on biopolymer-based soil treatment (BPST) technology in geotechnical engineering practices[J]. Transportation Geotechnics, 2020, 24: 100385.

[23] Jang J, Lee J, JUNG J. Characterization of agar for soil remediation[J]. Korean Society of Hazard Mitigation, 2017, 17(6): 351-358.

[24] Ayeldeen M, Negm A, El-Sawwaf M, et al. Enhancing mechanical behaviors of collapsible soil using two biopolymers[J]. Journal of Rock Mechanics and Geotechnical Engineering, 2017, 9(2): 329-339.

[25] Ryou J E, Lee J Y, Hong W T, et al. Effects of curing and soil type on unconfined compressive strengths and hydraulic conductivities of thermo-gelation biopolymer treated soils[J]. Construction and Building Materials, 2024, 432: 136493.

[26] Zhang X S, Wang H Y, Wang Y, et al. Improved methods, properties, applications and prospects of microbial induced carbonate precipitation (MICP) treated soil: a review[J]. Biogeotechnics, 2025, 3(1): 100123.

[27] Khatami H R, O'Kelly B C. Improving mechanical properties of sand using biopolymers[J]. Journal of Geotechnical and Geoenvironmental Engineering, 2013, 139(8): 1402-1406.

[28] Chang I, Prasidhi A K, Im J, et al. Soil strengthening using thermo-gelation biopolymers[J]. Construction and Building Materials, 2015, 77: 430-438.

[29] Smitha S, Rangaswamy K. Effect of biopolymer treatment on pore pressure response and dynamic properties of silty sand[J]. Journal of Materials in Civil Engineering, 2020, 32(8): 04020217.

[30] Affes R, Delenne J Y, Monerie Y, et al. Tensile strength and fracture of cemented granular aggregates[J]. The European Physical Journal E, 2012, 35(11): 117.

[31] Ge L, Hwang Y W, Sun H M, et al. Effective tensile strength of lightly cemented sand[J]. Journal of Materials in Civil Engineering, 2019, 31: 04018350.

[32] GB/T 50123—2019 Standard for geotechnical testing method [S].

[33] Chang I, Im J, Cho G C. Geotechnical engineering behaviors of gellan gum biopolymer treated sand[J]. Canadian Geotechnical Journal, 2016, 53(10): 1658-1670.

[34] Normand V, Lootens D L, Amici E, et al. New insight into agarose gel mechanical properties[J]. Biomacromolecules, 2000, 1(4): 730-738.

(编辑　XXX)